frontiers | Frontiers in Astronomy and Space Sciences

TYPE Original Research
PUBLISHED 06 July 2023
DOI 10.3389/fspas.2023.1201625

OPEN ACCESS

EDITED BY
Libo Liu,
Institute of Geology and Geophysics (CAS), China

REVIEWED BY
Bo Xiong,
North China Electric Power University, China
Jing Liu,
Shandong University, China

*CORRESPONDENCE
Attila Buzás,
buzas.attila@epss.hu

RECEIVED 06 April 2023
ACCEPTED 16 June 2023
PUBLISHED 06 July 2023

CITATION
Buzás A, Kouba D, Mielich J, Burešová D, Mošna Z, Koucká Knížová P and Barta V (2023), Investigating the effect of large solar flares on the ionosphere based on novel Digisonde data comparing three different methods.
Front. Astron. Space Sci. 10:1201625.
doi: 10.3389/fspas.2023.1201625

Investigating the effect of large solar flares on the ionosphere based on novel Digisonde data comparing three different methods

Attila Buzás[1,2,3]*, Daniel Kouba[4], Jens Mielich[5], Dalia Burešová[4], Zbyšek Mošna[4], Petra Koucká Knížová[4] and Veronika Barta[1]

[1]Institute of Earth Physics and Space Science (EPSS), Sopron, Hungary, [2]Doctoral School of Earth Sciences, Eötvös Loránd University, Budapest, Hungary, [3]ELKH-ELTE Space Research Group, Budapest, Hungary, [4]Department of Ionosphere and Aeronomy, Institute of Atmospheric Physics, Czech Academy of Sciences, Prague, Czechia, [5]Leibniz-Institute of Atmospheric Physics, Rostock, Germany

Increased solar radiation during solar flare events can cause additional ionization and enhanced absorption of the electromagnetic (EM) waves in the ionosphere leading to partial or even total radio fade-outs. In this study, the ionospheric response to large solar flares has been investigated using the ionosonde data from Juliusruh (54.63° N, 13.37° E), Průhonice (49.98° N, 14.55° E) and San Vito (40.6° N, 17.8° E) Digisonde (DPS-4D) stations. We studied the effect of 13 intense (>C4.8) solar flares that occurred between 06:00 and 16:30 (UT, daytime LT = UT+1 h) from 04 to 10 September 2017 using three different methods. A novel method based on the amplitude data of the measured EM waves is used to calculate and investigate the relative absorption changes (compared to quiet period) occurring during the flares. The amplitude data are compared with the variation of the *fmin* parameter (*fmin*, the minimum measured frequency, it is considered as a qualitative proxy for the "non-deviative" radio wave absorption). Furthermore, the signal-to-noise ratio (SNR) measured by the Digisondes was used as well to quantify and characterize the fade-out events and the ionospheric absorption. In order to compare the three different methods, residuals have been defined for all parameters, which provide the percentage changes compared to the selected reference periods. Total and partial radio fade-outs, increased values (+0.4%–318%) of the *fmin* parameter, and +20%–1400% amplitude changes (measured at 2.5 and 4 MHz) were experienced during and after the investigated flares. Generally, the observed changes depended on the intensity, solar zenith angle and duration of the flare events. Although the three different methods have their own advantages/disadvantages and their limitations, the combination of them seems to be an efficient approach to monitor the ionospheric response to solar flares.

KEYWORDS

space weather, solar flare, ionosphere, ionospheric absorption, ionosonde data, HF radio wave absorption, signal-to-noise ratio (SNR), radio fade-out

1 Introduction

The ionosphere is a region of Earth's atmosphere partially ionized mostly by the Sun. While the hard X-rays (<1 nm) of solar radiation penetrate deeper parts of the ionosphere, to the so-called D-region (60–90 km height), the soft X-ray (1–10 nm) and extreme UV flux (5–102.6 nm) reach higher layers (E-region 90–150 km and F-region above approximately 150 km) and cause ionization there (Rishbeth and Garriot, 1969; Zolesi and Cander, 2014). Solar energetic protons ionize the lower ionosphere (60–100 km) mainly in the polar regions.

The ionosphere influences propagation of electromagnetic (EM) waves depending on their frequency affecting the radio and satellite communication and navigation. The attenuation of EM waves propagating through the ionosphere is most significant in the high-frequency (HF) range (3–30 MHz), particularly important for radio wave communication (George and Bradley, 1973). The ionospheric absorption depends on the collisions between electrons and neutral molecules, thus on the collision frequency which strongly changes with altitude (Ratcliffe, 1972). The collision frequency is highest in the D-region (2×10^6 s^{-1}), therefore the radio waves below 10 MHz predominantly attenuate there (Zolesi and Cander, 2014). Like the electron density of the ionosphere (Bilitza et al., 2017) the ionospheric absorption also shows regular daily (maximum around local noon), seasonal (higher at summer, and a secondary maximum at winter) and solar cycle (increasing with higher solar activity) variation (Higashimura et al., 1969a; Higashimura et al., 1969b). Besides these phenomena, transient changes mainly related to solar activity can also occur in the ionosphere.

Solar flares are giant bursts taking place in the active regions on the Sun. During flares, huge amounts of EM energy are emitted at a broad range of wavelengths for a short period (~30 min to ~1 h) (Tsurutani et al., 2009). Solar flares are classified as large (X, >10^{-4} W/m^2), medium-size (M, ~10^{-5}–10^{-4} W/m^2) and small (C, ~10^{-6}–10^{-5} W/m^2) based on the released flux in 0.1–0.8 nm X-rays as measured on the GOES spacecraft. Furthermore, a finer logarithmic scale is also applied ranging from 0 to 9 within the above written classes. During flare events the enhanced radiation causes extra ionization and increased attenuation of the EM waves, leading to so-called short-wave fade-outs which last for tens of minutes or even hours (Rishbeth and Garriot, 1969; Davies, 1990; Tsurutani et al., 2009; Barta et al., 2019; Tao et al., 2020; Barta et al., 2022). Solar flares are also accompanied by energetic particles (protons and electrons from tens of keV to hundreds of MeV) propagating along the magnetic field lines, reaching the Earth at the polar region and causing further ionization and enhanced absorption there (Rishbeth and Garriot, 1969; Tsurutani et al., 2009). The so-called Polar Cap Absorptions following Solar Proton Events can last for even several days (Rose and Ziauddin, 1962). Moreover, recent studies (Liu et al., 2021a; Liu et al., 2021b) demonstrated that solar flare effects are not limited to the ionosphere where radiation energy is absorbed but they extend throughout the geospace via electrodynamic coupling: it causes changes in the dayside solar wind–magnetosphere interaction, causing less Joule heating of the upper atmosphere, leading to the reconfiguration of magnetosphere convection and changes in dayside and nightside auroral precipitation.

The abovementioned shortages and blackouts in radio communication can cause problems especially in commercial and military aircraft operations and affect the navigation systems. Therefore, detecting, modeling, and monitoring the ionospheric changes caused by solar flares became more important from day to day (Handzo et al., 2014; Barta et al., 2019). The theory of ionospheric absorption has been detailed by, e.g., Davies (1990), Sauer and Wilkinson (2008) and Scotto and Settimi (2014). The Absorption Prediction model (D-Region Absorption Prediction, D-RAP2, https://www.swpc.noaa.gov/products/d-region-absorption-predictions-d-rap) developed by the Space Weather Prediction Center (SWPC) is widely used to review the state of the ionospheric absorption globally.

The most common devices to determine the ionospheric absorption are the so-called riometers (Relative Ionospheric Opacity meter) which analyze the cosmic radio noise measured at certain frequencies (usually at the 20–50 MHz range) (Little, 1954). However, these instruments are generally installed at high geographic latitudes (>60°), thus, they mainly measure the ionospheric absorption variation caused by the energetic particle precipitations (Stauning, 1996).

Another method is to use the minimum reflection frequency, *fmin* parameter, recorded on the ionograms, which is the rough measure of the "non-deviative" radio wave absorption (Rishbeth and Gariot, 1969; Davies, 1990) and can be used as an index during high absorption changes. The "*fmin* method" was used to study the ionospheric absorption variation generated by geomagnetic storms (Oksman et al., 1981), by planetary waves (Schmitter, 2011) or by other sources (Kokourov et al., 2006) in the last decades. The absorption changes in the different continents caused by X-ray ionization due to solar flares were also investigated using the *fmin* method (e.g., Sharma et al., 2010; Sripathi et al., 2013; Nogueira et al., 2015; Denardini et al., 2016; Barta et al., 2019; Tao et al., 2020). The observed changes varied between 4 and 8 MHz (more than 100%) at the time of the X-class flares and 1–4 MHz (50%–150%) at the time of the M-class flares comparing to the reference quiet days at the lower-midlatitude, low-latitude and equatorial stations. The relative changes of the ionospheric absorption measured by the *fmin* method depended on the X-ray radiation intensity, but it also showed a solar zenith angle dependence (Barta et al., 2019; 2022). The disadvantage of this method is that the absolute absorption variation cannot be quantitatively determined because the *fmin* parameter also depends on the radar characteristics and the background radio-noise level.

Since nowadays data from many ionosonde stations are available from all over the globe (e.g., GIRO - Global Ionosphere Radio Observatory, https://giro.uml.edu/, Reinisch and Galkin, 2011), it can be worthwhile to develop a novel technique to determine the ionospheric absorption from the different properties of the reflected EM waves measured by the ionosondes. The signal-to-noise ratio (SNR) of radio waves obtained from ionograms during flares and comparing it with values derived from reference days was used by Curto et al. (2018) to study the impact of solar flares on ionospheric absorption. This SNR method has been improved by de Paula et al. (2022). They determined three constraints that a solar flare must accomplish to cause detectable

disturbances by the proposed method, taking into account the geoeffective hard X-ray irradiance, geoeffective hard X-ray radiant exposure and the solar altitude.

The main purpose of this study is to demonstrate a novel method calculating the ionospheric absorption from amplitude data measured by Digisondes (particularly DPS-4D ionosondes) and investigate its effectiveness during flare events. The shown method is based on the work of Sales (2011). The absorption changes determined by the "amplitude method" are compared with the *fmin* parameter and the signal-to-noise ratio measured by the same Digisondes during the same flare events. Following this introduction (Section 1—*Introduction*), the used data and the details of the three methods are described in Section 2 (*Data and methods*). The results coming from the different methods are detailed in Section 3 (*Results*) after which they are compared with each other and with published results from the literature in Section 4 (*Discussion*). Ultimately, the summary of the work and the concluding remarks are given in Section 5 (*Conclusion*).

2 Data and methods

Thirteen flare events have been selected for investigation that occurred between 04 and 10 September 2017, one of the most active periods of Solar Cycle 24 (e.g., Berdermann et al., 2018; Yasyukevich et al., 2018; Mosna et al., 2020, among others). The following criteria were applied during the selection of the flares: the Sun had to be above the horizon, therefore, the solar zenith angle (SZA) <90°; the X-ray class of the flare >C8 because we aimed to study the effectiveness of the presented methods during more intense solar flares. The most important properties of the selected flare events are displayed in Table 1.

Data measured at three different European Digisonde stations were used for the analysis since the solar zenith angle of the Sun at the time of the flare is very important regarding the ionospheric response. The selected stations (Juliusruh: 54.63° N, 13.37° E; Průhonice: 49.98° N, 14.55° E and San Vito: 40.6° N, 17.8° E; Figure 1) are located at similar longitude, however, their latitude is different. Juliusruh (JR) and San Vito (VT) stations operated with 5 min and 15 min time resolution, respectively. The sampling rates were 2 and 15 min at Průhonice (PQ) during the investigated periods. Since the time resolutions were different at the three stations, we were also able to investigate the importance of the sampling rate in regard to the detection of the ionospheric absorption changes. We investigated the variation of the *fmin* parameter, what is a rough measure of the "non-deviative" radio wave absorption. Furthermore, the critical frequencies of the F2 layer (*foF2*) and the sporadic E layer (*foEs*) have also been analyzed because they should also be taken into account during the study of the ionospheric absorption.

In Figure 2 we summarize the solar and geomagnetic activity during 04–10 September 2017. One can see that the investigated period is very complex. The X-class solar flares occurring on 06 September were followed by intense geomagnetic storms on 07 and 08 September as it can be seen in the *Kp* and *Dst* indices. The impact of the energetic particles is also significant as it is shown by the increased proton and electron flux and by the *AE* index. This study focuses on the ionospheric absorption changes which are mainly caused by the solar flares. Nevertheless, it is important to keep in mind the other solar and geomagnetic activities taking place parallelly for the interpretation of the results. The data from the GOES 13 and 15 satellites used to investigate the X-ray, solar proton and electron flux and the geomagnetic indices were available at the OmniWeb database (https://omniweb.gsfc.nasa.gov/ and https://omniweb.gsfc.nasa.gov/form/omni_min_def.html).

2.1 Amplitude method (Sales-absorption method)

Amplitude data of the reflected echoes recorded by the Digisondes were used to calculate the relative ionospheric absorption of EM waves according to the method proposed by G. Sales (Sales, 2011). This method (amplitude method or Sales-absorption method) is based on the Friis transmission formula (Friis, 1946). The Friis transmission equation is used in telecommunications engineering, and gives the power received by one antenna under idealized conditions given another antenna some distance away transmitting a known amount of power. The formula was derived in 1945 by Danish-American radio engineer Harald T. Friis. The decadic logarithmic form of the equation is as shown below (**Eq. 1**):

$$10\lg(L) = 10\lg(P_t G_t G_r) + 20\lg\left(\frac{\lambda}{4\pi 2h}\right) - 10\lg\left(P_r\right) \qquad (1)$$

where L is the loss term including, among other factors, the absorption (in W units); P_t is the power of the transmitted signal (in W units); G_t is the gain of the transmitter (unitless); G_r is the gain of the receiver (unitless); λ is the wavelength of the signal (in m units); h is the height of the reflection (in m units); and P_r is the power of the receiver (in W units). The term on the left side and the three terms on the right side are measured in dB. The known terms are λ, h, and P_r which are recorded by the Digisondes. Please note that further in the text and on the figures we denote $10\lg(L)$ simply as L and $10\lg(P_t G_t G_r)$ simply as $P_t G_t G_r$.

In order to determine the loss term (L), the $P_t G_t G_r$ product must be derived first using the Friis formula (**Eq. 1**). This is done in the case of every investigated station, and it is called the calibration of the Digisonde system. We selected nighttime (18–03 UT which is 19–04 LT (CET) in the winter and 20–05 LT (CEST) in the summer, i.e., between 27 March 2017 and 30 October 2017) data from quiet time periods (X-ray flux<1E-6 W/m^2) and assumed that the loss term (L) was negligible during those periods. Data from 173 quiet days in 2017 and 2018 were selected in total (Supplementary Table SA1 in the Supplementary Material). The calibration was performed in seven frequency ranges (2.5, 3, 3.5, 4, 4.5, 5, and 5.5 MHz ± 200 kHz, respectively). To minimize the effect of sporadic E-layer, only time periods when the critical frequency of the sporadic E-layer (*foEs*) was below 2.3 MHz, the lowest investigated frequency were retained. Please note that the *foEs* parameter was taken from automatically scaled data by the SAO-X (https://ulcar.uml.edu/SAO-X/SAO-X.html) software with a C-score> = 60 (C-score is

TABLE 1 Most important properties of the selected solar flares. The times are in UT. Source of the data is the Hinode flare catalog: https://hinode.isee.nagoya-u.ac.jp/flare_catalogue/.

Date	Start time	Peak time	End time	Duration (min)	Active region location	X-ray class
04 September 2017	11:54	12:22	14:00	126	S07W08	C8.3
04 September 2017	15:11	15:30	15:33	22	S06W13	M1.5
05 September 2017	4:33	4:53	5:07	34	S11W18	M3.2
05 September 2017	6:33	6:40	6:43	10	S82E08	M3.8
06 September 2017	8:57	9:10	9:17	20	S08W32	X2.2
06 September 2017	11:53	12:02	12:10	17	S09W34	X9.3
07 September 2017	9:35	9:54	11:28	113	S08W47	M1.4
07 September 2017	10:11	10:15	10:18	7	S07W46	M7.3
07 September 2017	14:20	14:36	14:55	35	S11W49	X1.3
08 September 2017	7:40	7:49	7:58	18	S10W57	M8.1
08 September 2017	15:09	15:47	16:04	55	S08W68	M2.9
09 September 2017	10:50	11:04	11:42	52	S14W74	M3.7
10 September 2017	15:35	16:06	16:31	56	S08W88	X8.2

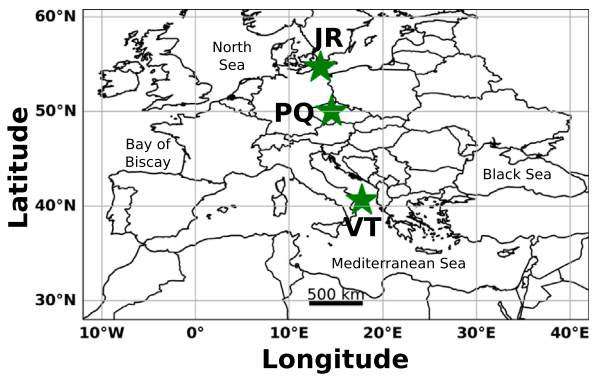

FIGURE 1
Location of the investigated DPS4D ionosonde stations in Europe. JR, Juliusruh; PQ, Průhonice; VT, San Vito.

a measure of the goodness of the automatic evaluation of the ionogram). Moreover, in certain periods at certain frequencies the number of data points at a given sounding can be very low because the echoes might not originate from an actual layer of the ionosphere but basically be generated by noise. Therefore, only soundings with more than 100 data points in each frequency range were retained during the calibration (Supplementary Figure SA1 in Supplementary Material). Only vertical echoes with ordinary polarization were selected, reflected from a height between 80 and 400 km (in order to avoid the second and third reflection of the F-layer). All the selected time periods and selection criteria used for the calibration are summarized in Supplementary Table SA1 in the Supplementary Material.

When assuming that the loss term is negligible, the $P_tG_tG_r$ product (or calibration function), which is characteristic for every Digisonde system depending on the actual technical settings of the measuring system, can be calculated from the Friis formula (Figure 3, **Eq. 2**).

$$10\lg(P_tG_tG_r) = 20\lg\left(\frac{4\pi 2h}{\lambda}\right) + 10\lg(P_r) \quad (2)$$

The values of the $P_tG_tG_r$ product lie in the interval of 150–170 dB at all three stations for the selected frequencies but the shapes of the curves generally differ from station to station (Figures 3A, C, E). The number of data points is the largest in the case of JR station as this station had a sampling rate of 5 min compared to the 15 min sampling rate of PQ and VT stations (Figures 3B, D, F). Moreover, at higher frequencies, i.e., above 3.5 MHz, the number of data points is considerably smaller. This is because the selected calibration periods are quiet, nighttime periods when reflections at higher frequencies occur less frequently which limits the usage of the Sales-absorption method.

After the calibration was performed, the Friis equation can be solved for the loss term which includes the ionospheric absorption relative to the quiet nighttime period (**Eq. 1**). The loss was determined at the abovementioned frequencies (2.5, 3, 3.5, 4, 4.5, 5, and 5.5 MHz ± 200 kHz, respectively) using some of the abovementioned selection criteria (vertical, ordinary echoes; foEs < 2.3 MHz; height of the reflection between 80 and 450 km) for the disturbed time period (04–10 September 2017).

Please note that in the case of PQ station the sampling rate was set from 15 to 2 min during the time period of 08 September 2017 08:40 UT–09 September 2017 21:00 UT which could possibly change (decrease) the sensitivity of the ionosonde due to shorter time of individual measurement. However, according to our analysis, this does not have any effect on the calculated absorption values as they do not display any step-like change around the time of the transitions of the 15–2 min and the 2–15 min periods (Supplementary Figure SA2 in Supplementary Material).

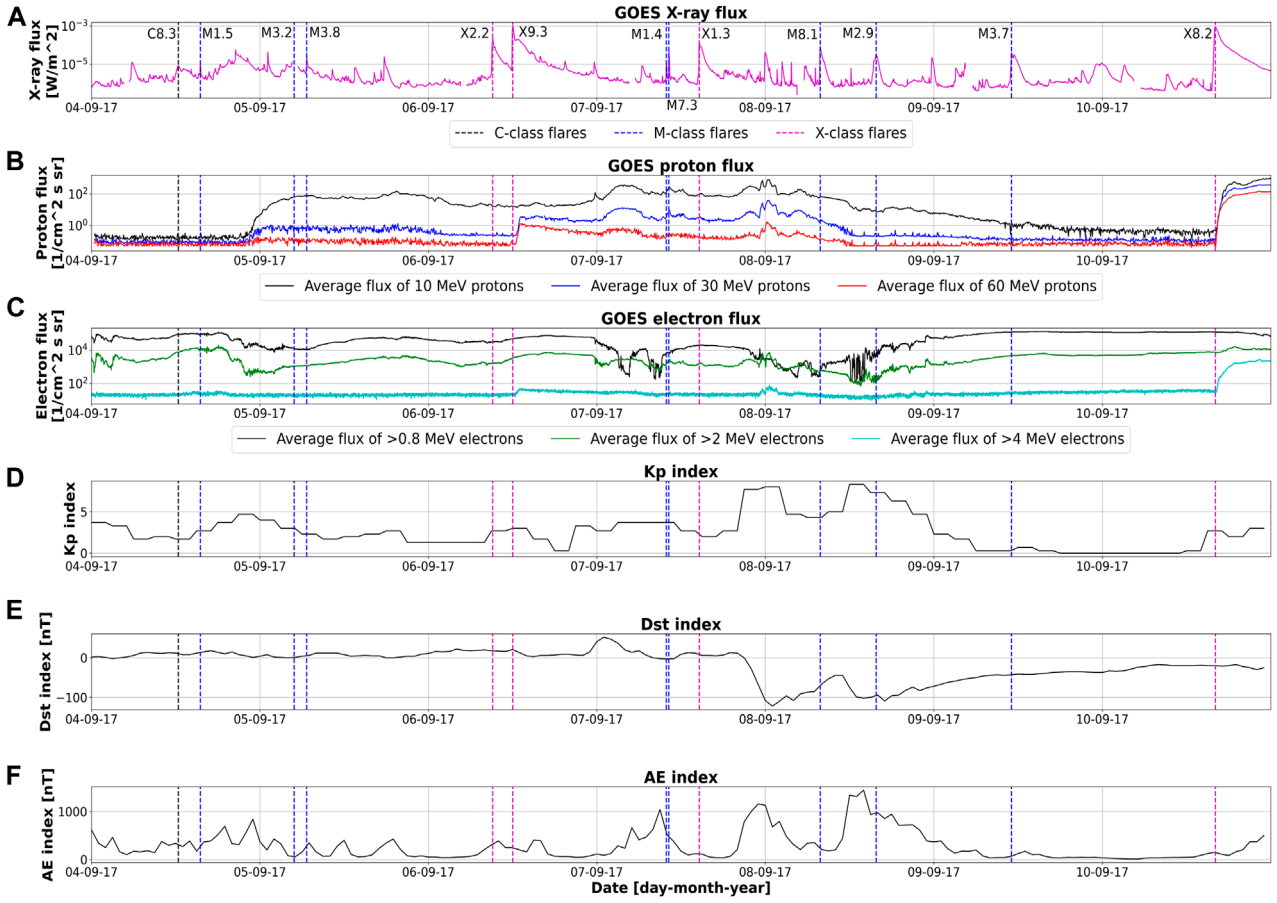

FIGURE 2
Summary of the solar and geomagnetic parameters for the investigated period. The class of the investigated flares are plotted on panel **(A)**. The black, blue and magenta dashed lines indicate C-, M- and X-class flares, respectively. The proton and electron fluxes measured in different energy ranges by the GOES spacecrafts are plotted on panels **(B,C)**, respectively. The variation of *Kp*, *Dst* and *AE* indices are displayed on panels **(D–F)**, respectively.

To evaluate the effect of solar flares on the ionosphere as seen in the absorption data, we determined the quiet diurnal variation of the absorption by calculating the loss term for the calibration period including not only nighttime data but data from all the day. Then we took the mean of the quiet diurnal variation in a time window of ±1 h around the peak time of the investigated flare (abs_{flare}). The absorption after the flare (abs_{flare}) was characterized by the maximum value of the absorption from a time window of the first valid measurement after the peak time of the flare (i.e., after fade-out if there is such) plus 1 h. The impact of the solar flare as seen in the absorption data was quantified by the equation below (**Eq. 3**):

$$\Delta abs = \frac{abs_{flare} - abs_{quiet}}{abs_{quiet}} \times 100[\%] \quad (3)$$

2.2 *fmin* method

The time series of the *fmin* parameter from the ionograms measured during the selected flare events have been analyzed. Since the *fmin* can depend on the radio-noise level and the radar characteristics, data recorded by three DPS-4D Digisondes were used to minimize the instrumental errors. To compare the observed changes measured by the different methods the residuals (relative changes in percentage compared to the reference days) have been defined using the following equation (**Eq. 4**):

$$\Delta fmin = \frac{fmin_{flare} - fmin_{quiet}}{fmin_{quiet}} \times 100[\%] \quad (4)$$

This formula was used in Barta et al. (2022) to investigate the *fmin* variation during flares. It is regularly used to analyze *foF2* parameter changes during geomagnetic storms in the literature (e.g., Buresova et al., 2014; Berényi et al., 2018). We used the same periods (X-ray < 1E-6) as for the Digisonde calibration as reference to the better comparison of the results coming from the two different methods (i.e., the amplitude and the *fmin* methods). It is worth mentioning that the value of the *fmin* parameter can also depend on the time resolution of the measurement at a certain station. The *fmin* parameter can be measured at lower frequencies (<2 MHz) during the standard 15 min settings because of the longer integration time than during high cadence campaigns, e.g., 2 min time resolution at

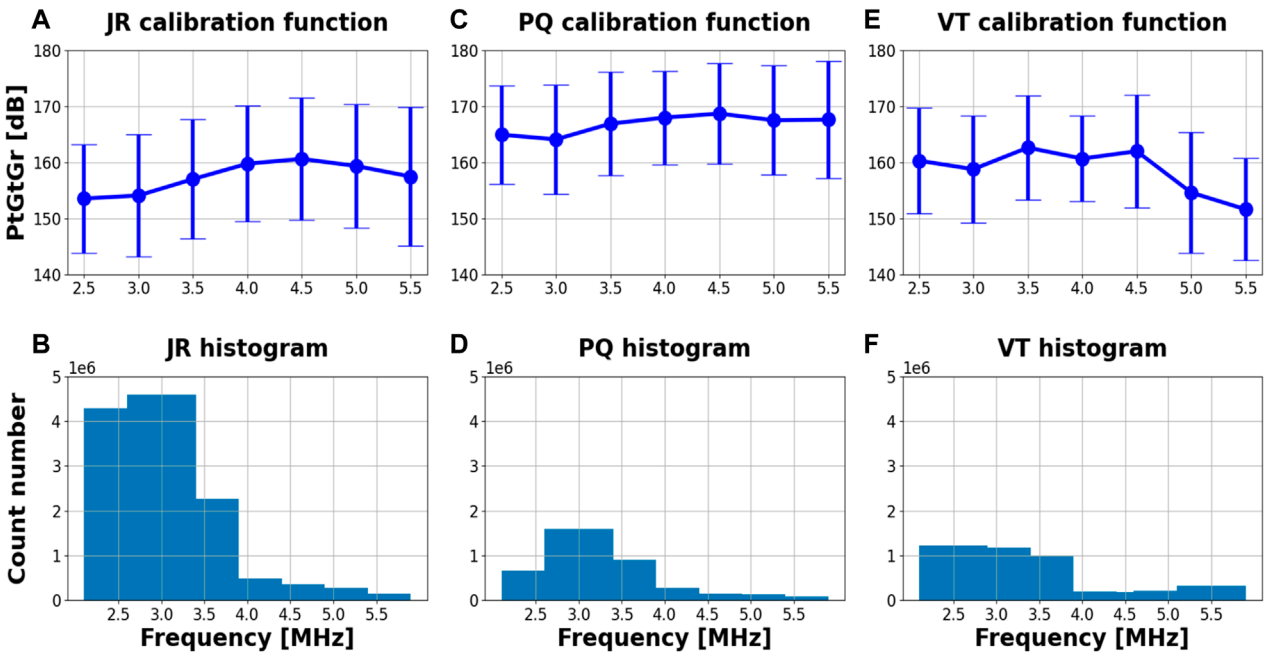

FIGURE 3
Calibration of the Digisonde systems at Juliusruh, Pruhonice, and San Vito (JR, PQ, and VT). Panels **(A,C,E)** show the PtGtGr product (calibration function) for the different stations, whereas the error bars represent two times the standard deviation of the data. The count number of the data used in the calibration in the different frequency ranges at the different stations are shown on panels **(B,D,F)**.

PQ station in some time periods in our case. During these campaign periods the ionograms started at 2, or 2.2 MHz at PQ, thus the traces (*fmin* parameter) was not detectable below these frequencies. Nevertheless, we focus on the impact of the solar flares in this study, when the *fmin* parameter is usually enhanced (e.g., Barta et al., 2019; 2022).

We also investigated the measured *foEs* and *foF2* parameters since their changes can indirectly affect the observed ionospheric absorption, especially in the case of the amplitude method. The ionograms used for our investigation were derived from the GIRO database and were processed and manually evaluated for the investigated period by the SAO-X program using the default 6 dB settings for MPA (most probable amplitude).

2.3 Signal-to-noise ratio

Modern Digisondes record data from which the signal-to-noise ratio (SNR) of the received signals can be derived. The SNR proved to be an efficient diagnostic tool for studying the effect of solar flares on the ionosphere and can visualize the absorption caused by the flares quite expressively (de Paula et al., 2022).

In the present study, we calculated the SNR from the amplitude data of the received echoes by using the following formula (**Eq. 5**):

$$SNR = Amp - MPA \tag{5}$$

Where Amp is the amplitude of the received signal in dB units and MPA is the so-called most probable amplitude which marks the amplitude threshold below the noise level recorded in dB units as well. Only vertical echoes with ordinary polarization were used in calculating the SNR without any constraints on the frequency or height.

To compare the disturbed period to a reference, we took the mean of five quiet days (X-ray < 1E-6) relatively close to the investigated time period (04–10 September 2017): 07, 16, 26 August 2017 and 16, 21 September 2017; and constructed a synthetic day from it. In the case of each flare, we selected data starting from the peak time of the flare until 1 h after the peak time of the flare. When the effect of the consecutive flare overlapped with the effect of the previous one, the end time of the selection window in the case of the first flare was the start time of the second flare. The percentage ratio of SNR values below 10 dB (including missing, i.e., Nan, values as well) and all the SNR values was calculated both in the case of the disturbed and in the case of the quiet time periods in the abovementioned time windows in the case of each flare (**Eq. 6**). The ratio calculated in the disturbed period in comparison to the one derived from the quiet period data is intended to show the impact of the solar flares.

$$SNR\,ratio = \frac{SNR_{below10dB}}{SNR_{all}} \times 100[\%] \tag{6}$$

3 Results

3.1 Amplitude method and *fmin*

3.1.1 Amplitude and ionosonde parameters variation during the whole investigated period

First, we show the amplitude and the ionospheric parameter changes for the whole investigated period (Figures 4, 5). The X-ray and proton flux changes measured by the GOES 13 and 15 satellites are seen in Figure 4 and Figure 5 panels (A) and (B). The peak time of the investigated flares are indicated by magenta dashed lines for X-class, blue dashed lines for M-class and black dashed line for the C8-class flare, respectively. Many intense flares occurred between 04 and 10 September. We only evaluated the events when the Sun was above the horizon at all the investigated stations. The absorption variation measured at 2.5 MHz at JR, PQ and VT stations are seen in Figures 4C–E, respectively. While the ionospheric parameters manually evaluated from the measured ionograms at the three stations are seen in Figures 4F–H. We show here the *fmin* parameter, as an indicator for the non-deviative radio wave absorption, and the *foEs* and *foF2* parameters which also can indirectly affect the measured amplitude values. The total radio fade-outs caused by the flares are determined based on the *fmin* parameter and are indicated by gray shaded areas. One can see that most of the X-class flares and some M-class flares lead to total blackout and the duration of the blackout decreases with the solar zenith angle.

Impact of the X-class flares can be clearly seen at 2.5 MHz at all stations. The changes can be easily tracked especially at JR because of the 5 min time resolution, and at PQ in the periods with 2 min time resolution. The X-class flares caused total radio fade-outs with longer duration and significantly increased values of the *fmin* at the lower midlatitude stations, especially at VT, thus the caused effect is more pronounced in the *fmin* parameter than in the amplitude data itself which is well observed for example on 10 September. One can see enhanced values of the amplitude data following the M-class flares, too. Comparing the data from the three stations during the same flares the *fmin* parameter shows a solar zenith angle dependence: the smaller the zenith angle of the station at the peak time of the flare the larger the *fmin* values. However, the latitude dependence of the amplitude data at 2.5 MHz is not evident especially during the more intense flares because they cause partial or total blackouts which can last for hours at the 2.5 MHz frequency band. The ionospheric response to the C8.3 class flare (peak time at 12:22 UT on 04 September) is also detectable both in the amplitude and in the *fmin* parameters at all three stations. The measured loss is larger at PQ than at JR, therefore it seems to show a latitude dependence. However, the *fmin* value increased above 5 MHz at VT at the peak time, which can explain that the amplitude change is not as large as measured at PQ. We can not exclude the effect of the energetic particles on the ionospheric absorption, especially at JR station which is located in the sub-auroral region. One can see a good example for that in the night of 08 September (around midnight) when there is an enhancement in proton flux (Figure 4B) and in parallel increased amplitude values at 2.5 MHz at JR (Figure 4C). Some enhanced values also appear at PQ at the same time (Figure 4D), but the impact is negligible at VT (Figure 4E) located at lower latitude. This variation of the absorption can not be tracked by the *fmin* parameter, which indicates that the amplitude method is more sensitive for the small changes. We will analyze the details focusing on some events in the following section.

Figure 5 shows the same parameters for the whole period as Figure 4 except that on panels (C), (D) and (E) one can see the absorption variation measured at 4 MHZ at the three stations (at JR, PQ and VT, respectively). The results are similar to the 2.5 MHz case. The amplitude measured at 4 MHz is enhanced at all stations after most of the X-class flares. The enhancement is especially pronounced after the X2.2 and X9.3 flares occurred on 06 September. The ionospheric changes connected to some X-class and the M-class flares are mostly detectable at JR station. It can be explained by the increased values of the *fmin* (>4 MHz) after those flares at PQ and particularly at VT, which means that there was no detectable amplitude data at 4 MHz at the peak time of the flares at these stations. Another interesting difference is what one can see between Figure 4 and Figure 5 is the effect caused by the C8.3 flare on 04 September. At 2.5 MHz the impact was detectable at all three stations, and it was the largest at PQ while at 4 MHz the caused effect is clearly seen only at VT. The impact caused by the energetic protons at JR during nighttime is even more pronounced at 4 MHz than in the previous case. Noticeably increased values are detected around midnight and in the early morning hours (01–03 UT) at 4 MHz at JR (Figure 5C) which is in good agreement with the periods of enhanced proton flux (Figure 5B). No similar effects were detected at 4 MHz at the other two stations during the same time intervals.

The increased values of the absorption (and data gap) detected at JR and PQ especially at 4 MHz during nighttime on 09 and 10 September are also worth mentioning. The reason for that can be the extremely low values of the *foF2* parameter measured at those stations in the nighttime on 09 and 10 September (Figures 5F, G). Consequently, as the 4 MHz frequency was not reflected, no valuable amplitude data were obtained. The impact of chosen individual flare events will be analyzed in detail in the following sections.

3.1.2 Amplitude and ionosonde parameters variation during one day

Figures 6, 7 demonstrate the variations of X-ray flux, proton flux, ionospheric absorption at 2.5 MHz (Figure 6) and at 4 MHz (Figure 7), and the ionospheric parameters at all three studied stations on 07 September, respectively. Two M-class flares (M1.4 and M7.3, peak times at 09:54 and at 10:15 UT, respectively) and an X1.3-class flare (peak time at 14:36 UT) occurred during the daytime, thus it is a good example to compare the impact of the flares on the different ionospheric parameters at the three stations. The duration of the two M-class flares is quite short, while the X-class flare took longer time as can be seen in the X-ray flux variation on Figure 6A, Figure 7A. The impact of the two M-class flares can be clearly seen on the *fmin* variation and on the amplitude changes measured at 4 MHz at JR. The caused effect is not so well tracked at the other two stations, there was a short radio blackout at PQ at the peak time of the M7.3 flare, while the *fmin* increased to ~7 MHz at VT at the same time. However, the impact of the two flares cannot be separated from each other at PQ and at VT. This case indicates that the time resolution of the ionosonde data is very important in studying the ionospheric response to solar flares. The 5 min resolution at JR provided enough information to track the effect of the M1.4 and M7.3 flares despite the

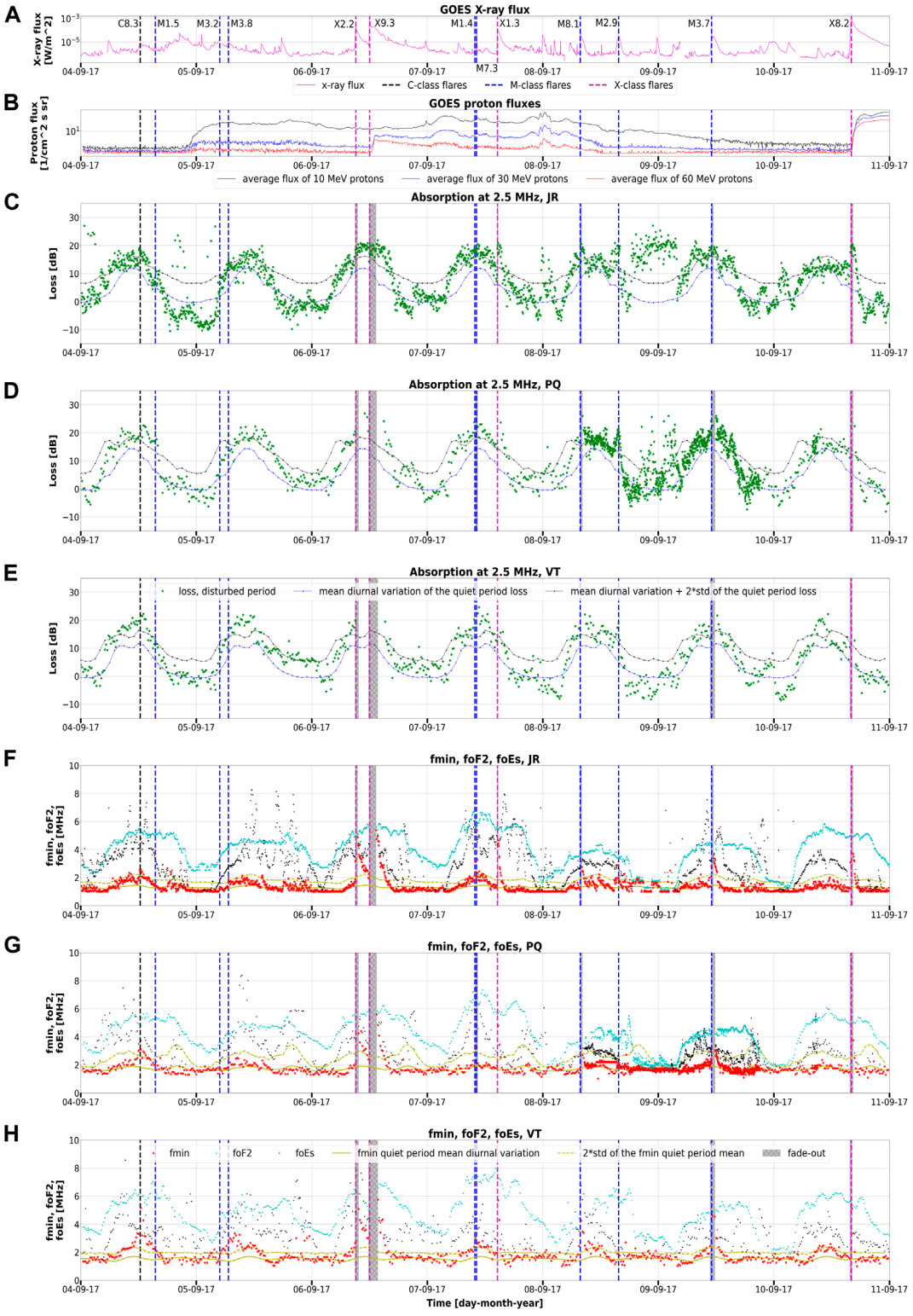

FIGURE 4
Overview of the investigated time period. Variation of X-ray flux **(A)**, proton flux **(B)**, ionospheric absorption at 2.5 MHz **(C–E)**, *fmin* (red dots), *foF2* (cyan dots) and *foEs* (black dots) parameters **(F–H)** at all three studied stations. The gray shaded areas denote the time periods of total absorption at a given frequency. The class of the investigated flares are plotted on panel **(A)**. The black, blue and magenta dashed lines indicate C-, M- and X-class flares, respectively.

10.3389/fspas.2023.1201625

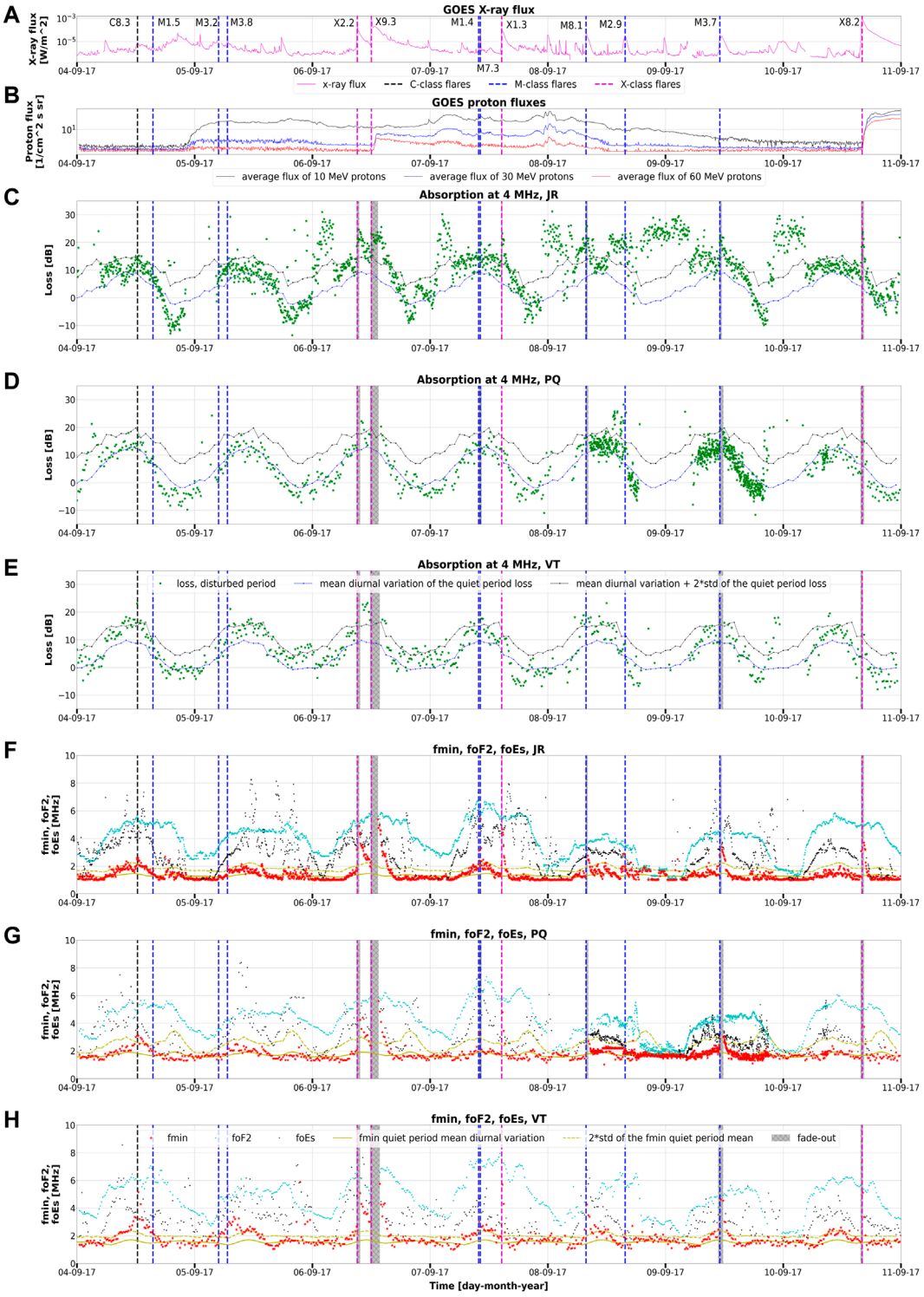

FIGURE 5
Overview of the investigated time period. Variation of X-ray flux **(A)**, proton flux **(B)**, ionospheric absorption at 4 MHz **(C–E)**, *fmin* (red dots), *foF2* (cyan dots) and *foEs* (black dots) parameters **(F–H)** at all three studied stations. The gray shaded areas denote the time periods of total absorption at a given frequency. The class of the investigated flares are plotted on panel **(A)**. The black, blue and magenta dashed lines indicate C-, M- and X-class flares, respectively.

10.3389/fspas.2023.1201625

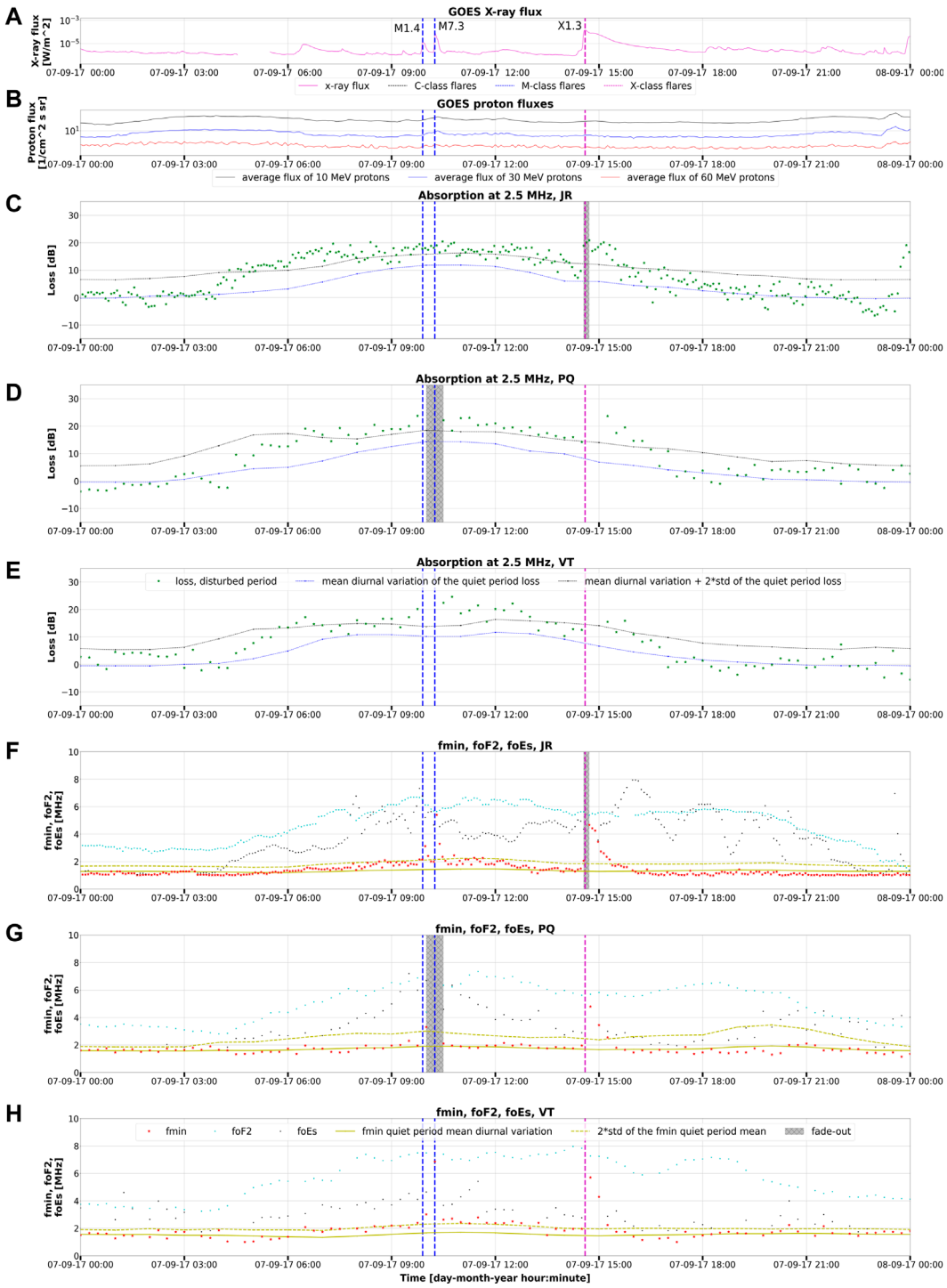

FIGURE 6
Variations of X-ray flux **(A)**, proton flux **(B)**, ionospheric absorption at 2.5 MHz **(C–E)**, *fmin*, *foF2* and *foEs* parameters **(F–H)** at all three studied stations on 07-09-2017. The time on the horizontal axes is in UT. The class of the investigated flares are plotted on panel **(A)**. The blue and magenta dashed lines indicate M- and X-class flares, respectively.

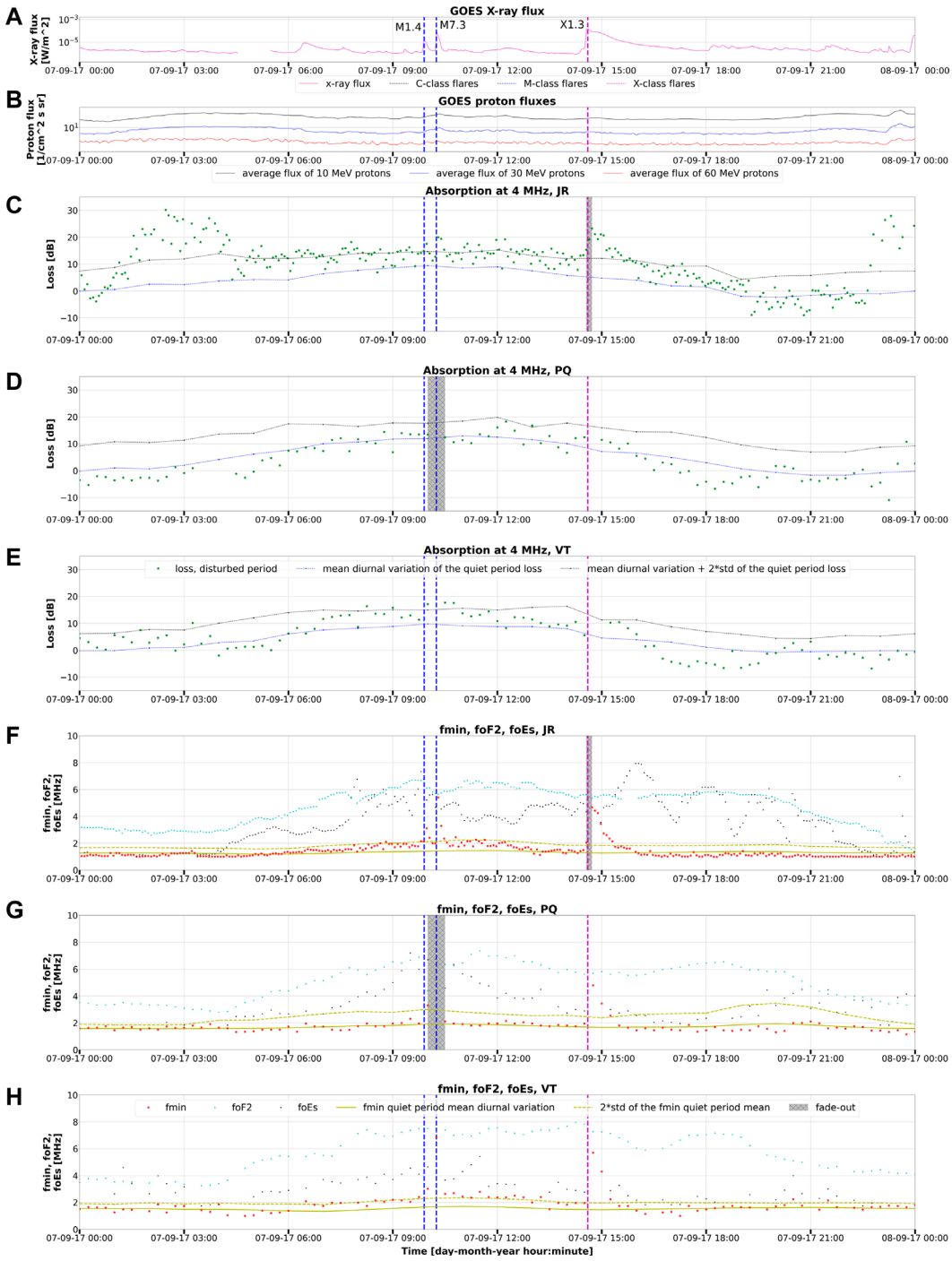

FIGURE 7
Variations of X-ray flux **(A)**, proton flux **(B)**, ionospheric absorption at 4 MHz **(C–E)**, *fmin*, *foF2* and *foEs* parameters **(F–H)** at all three studied stations on 07-09-2017. The time on the horizontal axes is in UT. The class of the investigated flares are plotted on panel **(A)**. The blue and magenta dashed lines indicate M- and X-class flares, respectively.

fact that the peak time of the second flare is only 20 min after the first one and the solar zenith angle was the largest at JR. In contrast, the data measured at every 15 min was not enough to detect the impact of these two flares separately at the other two stations because of the short lifetime of the events. The effect of the X1.3 flare is more apparent at all stations, mainly in the *fmin* at VT station, and in the amplitude at 2.5 MHz at JR and PQ. At 4 MHz, the change is only noticeable at JR (Figure 7C), but it can be explained by the high *fmin* parameter (>4 MHz) at the other two stations after the solar flare.

Two M-class flares occurred on 08 September, one in the morning hours (M8.1, peak time at 07:49 UT) and an M2.9 flare in the afternoon (peak time at 15:47 UT). The observed changes are seen on Figures 8, 9. Interestingly, the M8.1 flare caused total radio fade-out at JR and PQ, but not at VT. The *fmin* parameter was enhanced at all stations after this flare. One can see increased values of the amplitude at 2.5 MHz at JR and PQ (Figures 8C, D), while at VT there is a longer time without amplitude data at 2.5 MHz (Figure 8E) because the *fmin* was above this value here (Figure 8H). In contrast, the caused effect at 4 MHz loss is clearly detectable only at JR (Figure 9C), it is hard to recognize at the other two stations (Figures 9D, E).

The effect of the M2.9 (15:47 UT) flare is clearly seen in the amplitude data measured at 2.5 MHz at all stations (Figures 8C–E), but it is not that pronounced in the detected *fmin* parameters (Figures 8F–H). The caused impact can be tracked very well at PQ (Figure 8D) which station provided the data with 2 min time resolution during this period. This also strengthens that higher time resolution is very important to follow the changes generated by the solar flares. The caused impact is not that evident at the 4 MHz amplitude data measured at the different stations (Figures 9C–E), although it can be explained by the low values of the *foF2* parameter as its value was below 4 MHz at JR and PQ stations during this period.

The panels (D) on Figures 8, 9 show data from a high-rate ionogram campaign for PQ station (ionogram measurement every 2 min). Due to the duration of the ionogram measurement, the sounding frequency range had to be limited during this campaign. In the case of "full" ionograms measured every 15 min, the sounding starts at 1 MHz, but added ionogram soundings start at a higher frequency. From the beginning of the campaign (08:40 UT) until about 11 UT, the starting frequency was 2 MHz, between 11 and 14:30 UT it was 2.2 MHz, later again 2 MHz. Because the trace of the ionogram in these cases often starts at the first sounding frequency, so the *fmin* parameter must be lower than this frequency. These points are marked with less distinct symbols on the graph.

3.1.3 Amplitude and *fmin* parameter variation during the X2.2 flare on 06 September

The other way to demonstrate the results of the amplitude method is to investigate the loss detected at different frequencies at certain measurement times before and after the flare events. Here, we show the ionospheric response to the X2.2 flare on 06 September (Figure 10). The flare started at 08:57 UT and reached its peak at 09:10 UT as we can see in the GOES X-ray flux in the upper plots. Figures 10A–C show the data for JR, PQ and VT stations, respectively. The measured values of the *fmin* parameter at the different stations are seen in the second row, indicating the first, second, etc. measurements before and after the flare with red diamonds (the time of the record is also shown on the X-ray flux plots indicated by red diamonds too). The X2.2 solar flare caused total radio fade-out at all stations, its duration was 30 min at JR and 45 min at PQ and VT. The Digisonde operated with 5 min time resolution at JR and 15 min time resolution at PQ and VT. The *fmin* parameter was ~2 MHz at JR at 08:58 UT (second measurement before the flare), enhanced to ~3.2 MHz at 09:03 UT (first measurement before the flare) and returned with even higher values after the fade-out (4.9 MHz at 09:33 UT, 4.3 MHz at 09:38 UT and 4.2 MHz at 09:43 UT, first, second and third measurement after flare, respectively, Figure 10A). In the subplots showing the loss the blue stars (line) indicate the mean amplitude measured at different frequencies at the same time (from 08:57 UT to 09:48 UT from upper to lower at JR) during the reference periods, while the black stars (line) indicate the mean plus two times its standard deviation (SD). Generally, there are no increased amplitude values at JR at 08:57 UT (second measurement before flare), only the loss at 2.5 MHz and 4.5 MHz is at the values of the 2SD (2 standard deviation). However, the loss is increased (~20 dB) above the 2SD threshold at almost every frequency at 09:03 UT (first measurement before flare). We detected even more increased amplitude values (25 dB) at JR after the fadeout (at 09:33 UT, 09:38 UT and 09:43 UT first, second and third measurement after flare, respectively). The measured values reached the threshold even ~40 min after the peak time of the flare. The same plots for PQ station can be seen in Figure 10B. The *fmin* is ~2 MHz at the second (08:45 UT) and first (09:00 UT) measurements before the peak time of the flare. Its values increased and stayed around 4 MHz at the first (09:45 UT), second (10:00 UT) and third (10:15 UT) measurement after the flare. The amplitude data are above the 2SD threshold only at lower frequencies (2.5 and 3 MHz) before the peak of the flare. There is only one data (point) at 4.5 MHz at 09:45 UT (first measurement after the flare) because of the partial fade-out. Increased amplitudes were observed at 3.5 and 4 MHz at 10:00 UT and 10:15 UT (second and third measurement after flare, still no record at 2.5 and 3 MHz). We still detected enhanced loss at 3.0–4.5 MHz at 10:30 UT, 80 min after the peak time of the flare. The observed effect is even more pronounced at VT (Figure 10C). The *fmin* parameter is 2.3 MHz at 08:45 UT and 2.7 MHz at 09:00 UT (second and first measurement before the peak time of the flare). After the 45 min long total radio fade-out the *fmin* returns with 5.1 MHz at 09:45 UT (first measurement after flare) and it changes to 4.3, 4.1, and 3.6 MHz at 10:00 UT, 10:15 UT and 10:30 UT (second, third and fourth measurement after flare respectively). The decreasing trend of the *fmin* seems to agree well with the GOES X-ray flux variation in the upper plot. We observed increased amplitude values at 2.5–4.5 MHz frequency range even before the peak of the flare (at 09:00 UT). The partial fade-out is very remarkable in the amplitude data display, too. No reflections were detected in the first and second measurement after the flare (09:45 UT and 10:00 UT) in the 2.5–4 MHz band. Furthermore, the partial fade-out (no data in the lower frequency range: 2.5–3 MHz) took place until the start of the next flare (11:53 UT). The detected loss values were above the threshold at every frequency, with especially increased values at 10:00 UT and 10:15 UT (second and third measurement after flare).

3.2 Signal-to-noise ratio analysis

The impact of the solar flares can be investigated also using the signal to noise ratio (SNR) measured by the Digisondes (Curto et al., 2018; de Paula et al., 2022). Here we demonstrate the SNR observed on 06 September 2017 when two large flares occurred (X2.2, peak time: 09:10 UR and X9.3, peak time: 12:02 UT) comparing it to a mean reference day derived from five individual days (07, 16, 26

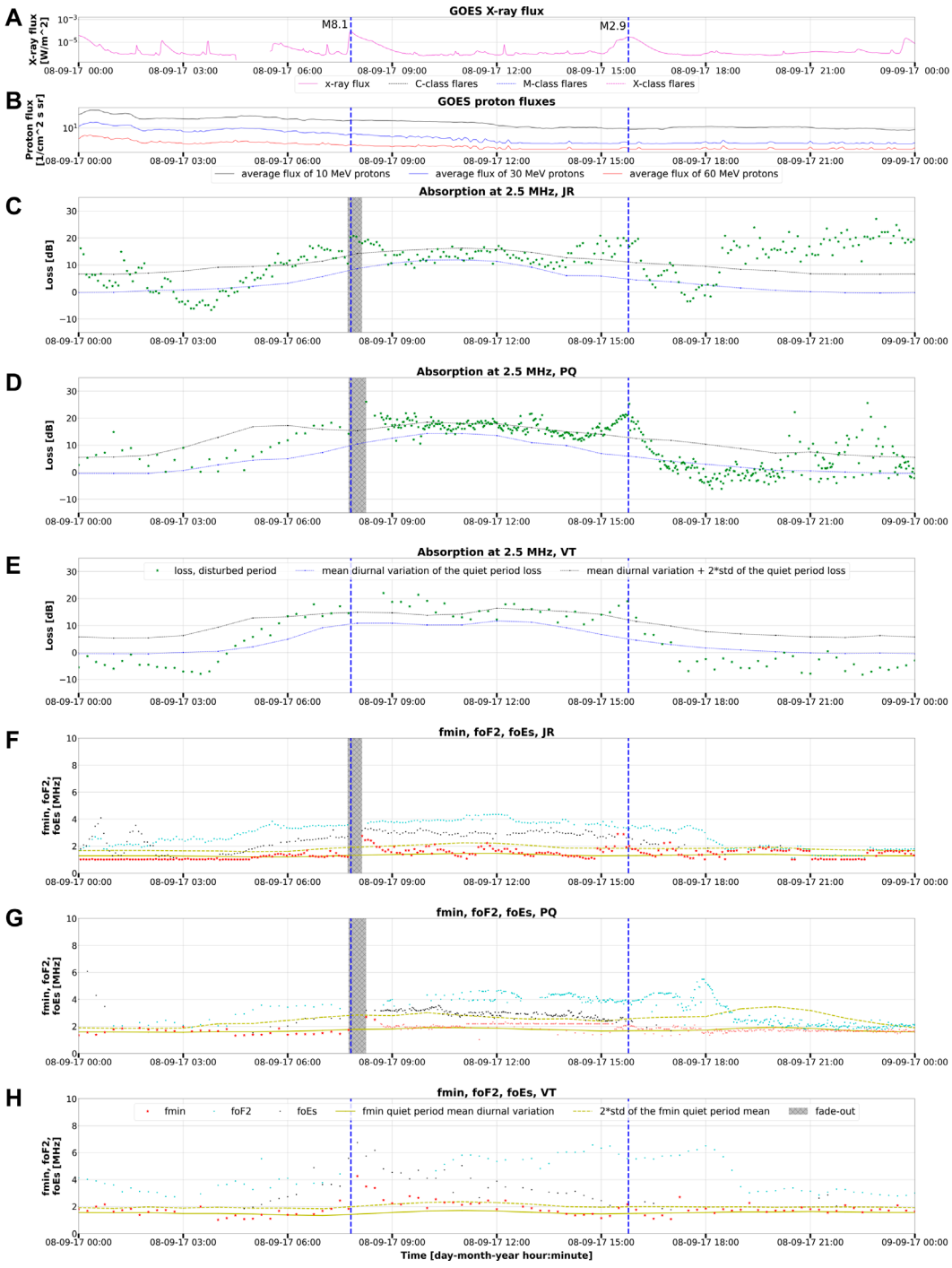

FIGURE 8
Variations of X-ray flux **(A)**, proton flux **(B)**, ionospheric absorption at 2.5 MHz **(C–E)**, *fmin*, *foF2* and *foEs* parameters **(F–H)** at all three studied stations on 08-09-2017. The time on the horizontal axes is in UT. The class of the investigated flares are plotted on panel **(A)**. The blue dashed lines indicate M-class flares.

August 2017 and 16, 21 September 2017; Figure 11). We used the same reference period for the three stations. Looking through the plots of reference days one can see that the diurnal variation of the SNR is a bit different at the three stations. The larger *fmin* values around noon were detected at VT, the highest observed frequencies (*foF2*) reached the highest values also at VT (above 8 MHz from 06:00 to 24:00 UT), above 7 MHz at JR (between 06:00 and 24:00 UT) and only 6–7 MHz at PQ. The total radio fade-outs caused by the two large solar flares are very well pronounced in the SNR tables of the three stations with the large empty territories after their time of occurrence (indicated by magenta lines). The restricted frequencies are also seen as white horizontal lines especially at VT.

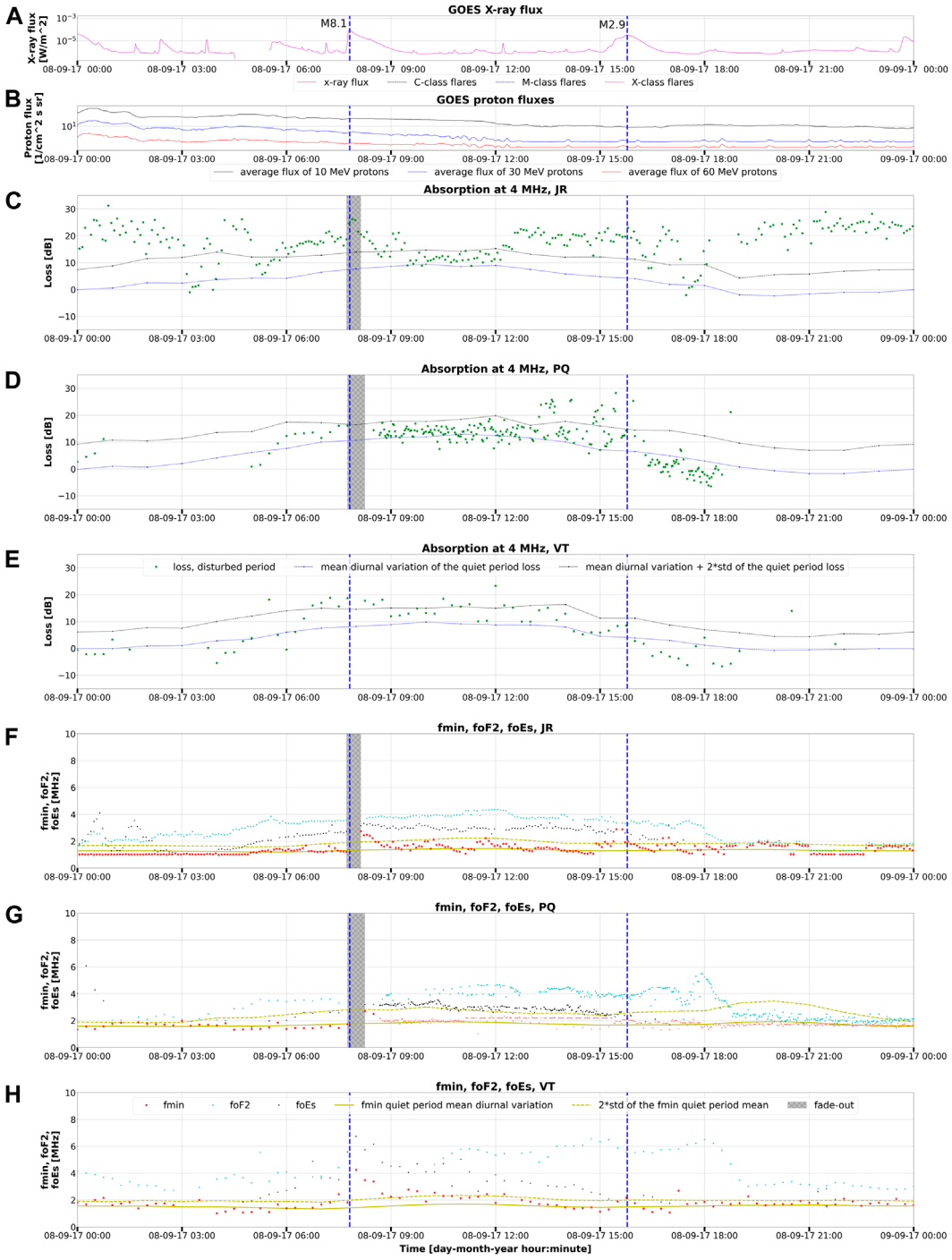

FIGURE 9
Variations of X-ray flux **(A)**, proton flux **(B)**, ionospheric absorption at 4 MHz **(C–E)**, *fmin*, *foF2* and *foEs* parameters **(F–H)** at all three studied stations on 08-09-2017. The time on the horizontal axes is in UT. The class of the investigated flares are plotted on panel **(A)**. The blue dashed lines indicate M-class flares.

4 Discussion

This study demonstrates a novel method to calculate the ionospheric absorption from amplitude data measured by the Digisondes. The amplitude method was introduced by Sales (2011), but it has not been applied to investigate the impact of multiple solar flares and it has not been compared with other methods to measure the ionospheric absorption, yet. One of the main objectives of this study is to fill this gap, namely, to study the solar flare effects on the ionospheric absorption by the amplitude method and to compare it with the *fmin* parameter and the signal-to-noise ratio measured by the same Digisonde during the same events. We

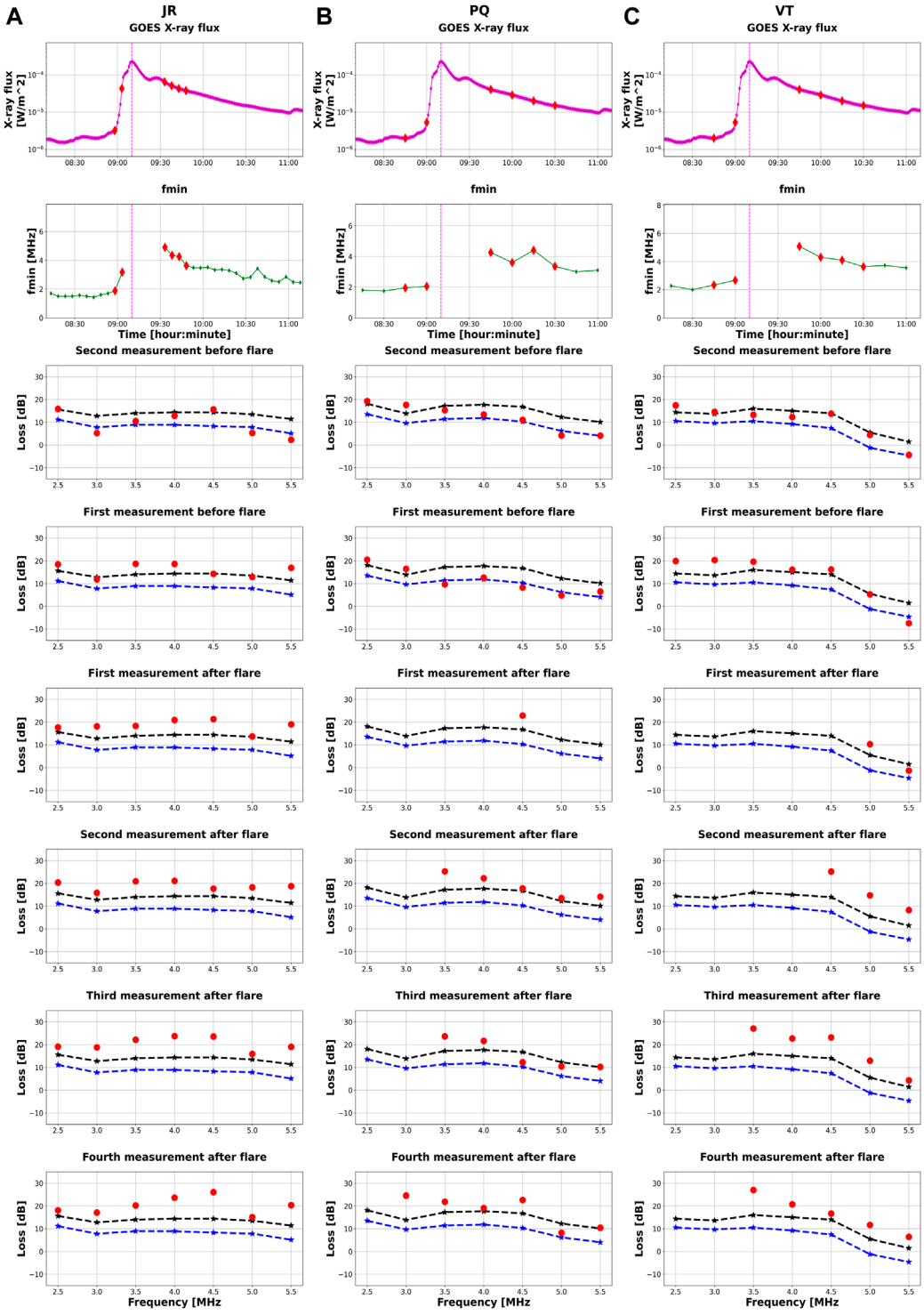

FIGURE 10
The effect of the X2.2 flare on 06 September 2017 in the *fmin* and absorption data at JR **(A)**, PQ **(B)** and VT **(C)** stations at all the investigated frequencies. The first measurement after the investigated flare (and the fade-out if there was any) was performed at 09:33:16 (in UT, at JR station with a sampling rate of 5 min) and at 09:45:00 UT (PQ, VT with a sampling rate of 15 min). The times on the plots in the upper two rows are in UT. The blue and black lines and the red dots denote the quiet period mean of the absorption, the quiet period mean plus 2 times the standard deviation of the absorption and the actual values of the absorption, respectively. Red diamonds on the panels in the upper two rows denote the second and first measurements before the flare and the first, second, third and fourth measurements after the flare. The magenta dashed lines on the upper two rows indicate the time of the flare.

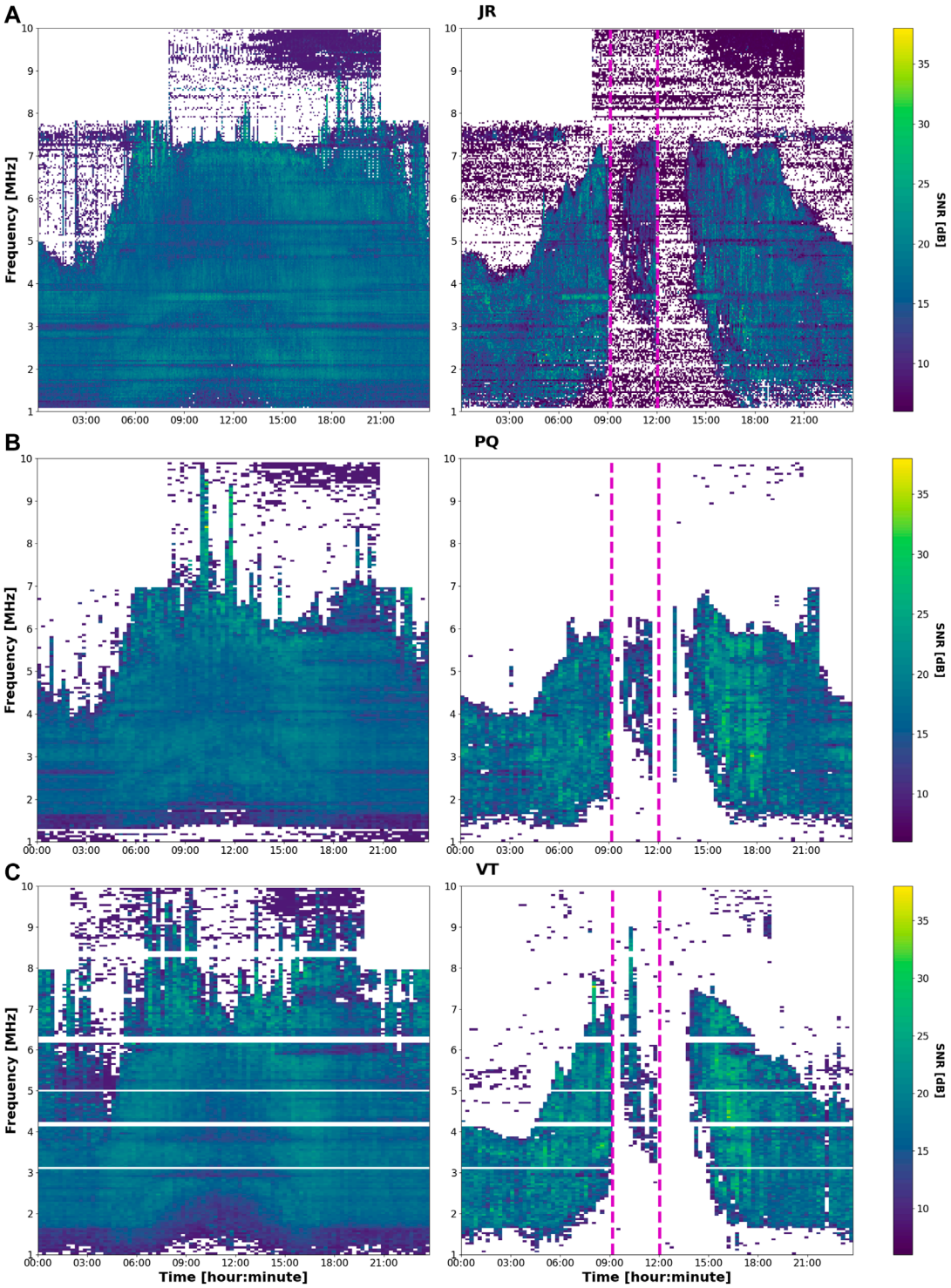

FIGURE 11
Demonstration of the SNR method. On the left, mean SNR taken from five quiet days (07, 16, 26 August 2017 and 16, 21 September 2017) are plotted, whereas on the right data from the disturbed period (06 September 2017) are displayed showing the effect of two X-class flares (vertical dashed magenta lines). The time on the horizontal axes is in UT. Panels **(A–C)** show the data for JR, PQ and VT stations, respectively.

selected thirteen intense solar flares (>C8) from the very active period of 04 and 10 September 2017 for investigation. In order to compare the three methods used for the analysis of the ionospheric absorption variation, residuals have been defined for all parameters, which provide the percentage changes compared to the selected reference periods. The exact determination of the residuals and the used reference periods are detailed in the Data and methods section (Section 2). The changes detected by different methods at JR, PQ and VT stations are shown in Tables 2–4, respectively. In order to help the careful comparison of the impact of the different flares we also added the following columns to Tables 2–4: "Time of first measurement after flare" and "X-ray flux at the time of the first measurement after flare." Because of the total radio fade-out we do not have observed values at the peak time of the larger flares, thus, the first observation happens at a later time, when the X-ray flux is decreased compared to the peak time. If one would like to compare the recorded values and ionospheric changes, it is better to take into account the X-ray flux at the exact time of the observation, than only the class of the flare itself.

The percentage change measured at the three stations after the flares was between +68% to +1430%, −50% to +565% and +0.4% to +318% in the case of the absorption method at 2.5, at 4 MHz and in the case of the *fmin* method, respectively. The ratio of small (<10 dB) and missing values in the case of the SNR method was between 1% and 100% (the maximum value is 100% in this case). The residuals with the largest fluctuations were produced by the absorption method, even indicating a reduction after the flare (−50% in the case of the M2.9 flare with peak time at 15:47 UT on 09 September at 4 MHz at VT). The largest enhancement in the absorption values at 2.5 MHz was after the M3.2 flare (peak time at 4:53 UT) on 05 September at all three stations. However, at 4 MHz the situation is more complex, as the largest increase in the absorption at this frequency was after the X8.2 flare (peak time at 16:06 UT) on 10 September, the M2.9 flare (peak time at 15:47 UT) on 08 September and the M3.2 flare (peak time at 4:53 UT) on 05 September at JR, PQ and VT stations, respectively. Nonetheless, it is important to note that the longest duration of fade-out happened after the largest, X9.3 flare (peak time at 12:02 UT) on 06 September in the case of all three stations and the percentage residuals can not be calculated in the case of fade-out as there are no data present to calculate the absorption. The largest enhancement in the *fmin* values was caused by the X9.3 flare on 06 September in the cases of JR and PQ stations but it happened after the M7.3 flare (peak time at 10:15 UT) on the 07 September in the case of VT station. The duration of the fade-out may have impacted the percentage residuals in the case of the *fmin* data as well. The ratio of missing and small values of the SNR reached its maximum value (100%) after the X9.3 class flare on 06 September in the cases of JR and PQ and it reached 100% after three flares [the two X-class flares on 06 September and the M3.7 flare (peak time at 11:04 UT) on 10 September] at VT station.

The amplitude changes measured at 2.5 MHz can be mainly related to the enhanced absorption occurring in the D-layer, since the signals are reflected generally from the E-layer at 90–130 km height (or from the Es-layer) at this frequency range during daytime. The observed changes at 2.5 MHz varied between 68% and 740% at JR, 75% and 363% at PQ and 76% and 1430% at VT, respectively. Basically, the ground-based VLF measurements are commonly used to monitor the changes of the D-layer after solar flares (e.g., Šulić and Srećković, 2014; Srećković et al., 2021; Kolarski et al., 2023). The electron density profile (Ne) can be determined by the measured amplitude and phase changes using a trial-and-error method where Ne is modified until the LWPC (Long Wave Propagation Capability model, available online: https://github.com/space-physics/LWPC) computed parameters (Šulić et al., 2016) are agreed with the detected ones (Srećković et al., 2021). The latter study also analyzed the impact of the M3.7 flare (peak time at 11:04 UT on 09 September) and they found that the electron density increased at reference height h = 74 km from 2.2×10^8 m^{-3} to 6.7×10^{10} m^{-3}, thus about with two orders of magnitude. We observed 67% (at JR), 85% (at PQ) and 103% (at VT) changes at 2.5 MHz after the same flare, thus the magnitude of the detected changes by the absorption method does not agree with the calculated Ne changes from the VLF data. Although it is important to mention that the M3.7 class flare caused total radio fade-out (30–48 min) at all stations, therefore there was no measured data at the peak time of the flare. According to the results of Kolarski et al. (2023) the electron density (at midlatitude) increased by almost three and about 3.5 orders of magnitude at 74 km after the X2.2 and X9.3 flares on 06 September, respectively. This is a very large value compared to the changes (77%–116%) detected at 2.5 MHz at the ionosonde stations after the same flare. However, these large flares caused long-lasting total radio blackouts at all stations, thus we had detected signals only 30–120 min after the peak time. Nevertheless, the computed Ne changes are ~100% at 74 km after C4.8–C5.1 class flares (Srećković et al., 2021; Barta et al., 2022) which agree with the changes (68%–102%) observed at 2.5 MHz after the C8.3 flare on 04 September, when there was no total radio blackout.

The amplitude changes measured at 4 MHz indicate also the changes of the absorption in the E-region beside the D-layer. We detected 82%–565% (at JR), 18%–222% (at PQ) and 66%–273% (at VT) changes at this frequency range during and after the investigated flare events. The most intense (X9.3) investigated flare caused 96%–174% changes at 4 MHz at the different stations. The impact of the same flare on the ionosphere was investigated also by Incoherent Scatter Radar measurements. Liu et al. (2022) showed that electron density in the E-region (mainly below 150 km) increased by ~$7{\cdot}10^{10}$ m^{-3} over Millstone Hill (42.6°N), a midlatitude/sub-auroral station in the American sector. Furthermore, Liu et al. (2021b) used EISCAT (European Incoherent SCATter) radar data and found that the induced electron density and temperature changes in the E-region are very well pronounced even at high latitudes (69°–72°N). Chen et al. (2021) used numerical modeling to investigate the effect of the X9.3 (06 September) and X8.2 (10 September) flares on the ionosphere and found that at the flare peak, not only the electron and temperature increased but also the E-region conductivity which causes further electrodynamic responses. Barta et al. (2022) found a 0.5–0.7 MHz enhancement of the *foE* parameter (critical frequency of E-region) compared to the reference days at PQ and VT stations after an M6 flare. Furthermore, Sharma et al. (2010) detected increased values (by 0.5 MHz) of the *foE* at Ahmedabad (India) low latitude station after the flare occurred on 12 May 1997. In terms of electron density of the E-region peak it means a ~30% enhancement, which is smaller than the observed changes at 4 MHz (as seen above). Consequently, the absorption variations within the

TABLE 2 Overview of the effect of the flares on the ionosphere as seen by all three studied methods at JR station. For the calculation method of change in absorption please refer to Section 2.1, for the change in *fmin* Section 2.2, and for the SNR ratios Section 2.3. All the times in the table are listed in UT.

JR									
Flares (peak time and class)	SZA	Time of first measurement after flare	X-ray flux at the time of the first measurement after flare	Change in absorption at 2.5 MHz	Change in absorption at 4 MHz	Change in *fmin*	Duration of total fade-out	SNR ratio, disturbed period (%)	SNR ratio, quiet period (%)
09.04.17 12:22 C8.3	50.03°	09.04.17 12:23	8.1e-6 Wm^{-2}	+68%	+82%	+73%	—	11	0
09.04.17 15:30 M1.5	70.62°	09.04.17 15:33	8.3e-6 Wm^{-2}	+103%	+53%	+31%	—	1	0
09.05.17 4:53 M3.2	86.07°	09.05.17 4:53	NaN	+740%	+233%	+0.4%	—	43	11
09.05.17 6:40 M3.8	70.91°	09.05.17 6:43	1.8e-5 Wm^{-2}	+326%	+492%	+65%	—	37	0
09.06.17 9:10 X2.2	53.53°	09.06.17 9:33	6.5e-5 Wm^{-2}	+102%	+188%	+258%	30 min	94	0
09.06.17 12:02 X9.3	49.07°	09.06.17 13:23	1.3e-4 Wm^{-2}	+92%	+174%	+275%	90 min	100	0
09.07.17 9:54 M1.4	50.72°	09.07.17 9:58	8e-6 Wm^{-2}	+97%	+134%	+128%	—	28	0
09.07.17 10:15 M7.3	49.71°	09.07.17 10:18	3.6e-5 Wm^{-2}	+79%	+127%	+283%	—	32	0
09.07.17 14:36 X1.3	64.47°	09.07.17 14:43	8.5e-5 Wm^{-2}	+197%	+287%	+252%	10 min	47	0
09.08.17 7:49 M8.1	62.67°	09.08.17 8:08	2.3e-5 Wm^{-2}	+256%	+329%	+119%	25 min	82	0
09.08.17 15:47 M2.9	74.42°	09.08.17 15:48	3e-5 Wm^{-2}	+262%	+378%	+55%	—	77	0
09.09.17 11:04 M3.7	49.46°	09.09.17 11:28	3e-5 Wm^{-2}	+67%	+152%	+135%	30 min	86	0
09.10.17 16:06 X8.2	77.83°	09.10.17 16:28	4.7e-4 Wm^{-2}	+335%	+565%	+185%	35 min	61	0

TABLE 3 Overview of the effect of the flares on the ionosphere as seen by all three studied methods at PQ station. For the calculation method of change in absorption please refer to Section 2.1, for the change in *fmin* Section 2.2, and for the SNR ratios Section 2.3. All the times in the table are listed in UT.

PQ									
Flares (peak time and class)	SZA	Time of first measurement after flare	X-ray flux at the time of the first measurement after flare	Change in absorption at 2.5 MHz	Change in absorption at 4 MHz	Change in *fmin*	Duration of total fade-out	SNR ratio, disturbed period (%)	SNR ratio, quiet period (%)
09.04.17 12:22 C8.3	46.2°	09.04.17 12:30	7e-6 Wm^{-2}	+75%	+35%	+68%	—	9	0
09.04.17 15:30 M1.5	70.15°	09.04.17 15:30	1.5e-5 Wm^{-2}	+171%	+18%	+18%	—	4	0
09.05.17 4:53 M3.2	85.86°	09.05.17 5:00	NaN	+363%	+154%	+9%	—	36	0
09.05.17 6:40 M3.8	68.97°	09.05.17 6:45	1.3e-5 Wm^{-2}	+241%	+68%	+53%	—	30	0
09.06.17 9:10 X2.2	49.38°	09.06.17 9:45	4.1e-5 Wm^{-2}	+116%	+95%	+132%	45 min	80	0
09.06.17 12:02 X9.3	45.59°	09.06.17 13:30	1.1e-4 Wm^{-2}	+86%	+65%	+203%	105 min	100	0
09.07.17 9:54 M1.4	46.16°	09.07.17 10:00	4.1e-6 Wm^{-2}	+85%	+17%	+80%	—	25	0
09.07.17 10:15 M7.3	45.04°	09.07.17 10:30	1.6e-6 Wm^{-2}	+68%	+11%	+12%	30 min	23	0
09.07.17 14:36 X1.3	63.01°	09.07.17 14:45	8e-5 Wm^{-2}	+156%	+20%	+179%	—	38	0
09.08.17 7:49 M8.1	59.59°	09.08.17 8:15	1.7e-5 Wm^{-2}	+243%	+82%	+59%	30 min	80	0
09.08.17 15:47 M2.9	74.19°	09.08.17 15:48	3e-5 Wm^{-2}	+237%	+222%	+27%	—	37	0
09.09.17 11:04 M3.7	44.83°	09.09.17 11:48	1.6e-5 Wm^{-2}	+85%	+56%	+59%	48 min	98	0
09.10.17 16:06 X8.2	77.89°	09.10.17 16:30	4.3e-4 Wm^{-2}	+303%	+142%	+124%	45 min	45	0

TABLE 4 Overview of the effect of the flares on the ionosphere as seen by all three studied methods at VT station. For the calculation method of change in absorption please refer to Section 2.1, for the change in *fmin* Section 2.2, and for the SNR ratios Section 2.3. All the times in the table are listed in UT.

VT									
Flares (peak time and class)	SZA	Time of first measurement after flare	X-ray flux at the time of the first measurement after flare	Change in absorption at 2.5 MHz	Change in absorption at 4 MHz	Change in *fmin*	Duration of total fade-out	SNR ratio, disturbed period (%)	SNR ratio, quiet period (%)
09.04.17 12:22 C8.3	39.62°	09.04.17 12:30	7e-6 Wm^{-2}	+102%	+91%	+213%	—	56	6
09.04.17 15:30 M1.5	70.72°	09.04.17 15:30	1.5e-5 Wm^{-2}	+89%	+66%	+62%	—	7	6
09.05.17 4:53 M3.2	84.43°	09.05.17 5:00	NaN	+1430%	+309%	+33%	—	12	6
09.05.17 6:40 M3.8	64.4°	09.05.17 6:45	1.3e-5 Wm^{-2}	+269%	+273%	+100%	—	17	6
09.06.17 9:10 X2.2	40.58°	09.06.17 9:45	4.1e-5 Wm^{-2}	+83%	+161%	+227%	45 min	100	6
09.06.17 12:02 X9.3	38.2°	09.06.17 13:45	8.7e-5 Wm^{-2}	+77%	+96%	+249%	120 min	100	6
09.07.17 9:54 M1.4	36.63°	09.07.17 10:00	4.1e-6 Wm^{-2}	+132%	+98%	+95%	—	41	6
09.07.17 10:15 M7.3	35.4°	09.07.17 10:15	8e-5 Wm^{-2}	+136%	+92%	+318%	—	40	6
09.07.17 14:36 X1.3	61.67°	09.07.17 14:45	8e-5 Wm^{-2}	+76%	+47%	+280%	—	49	6
09.08.17 7:49 M8.1	52.86°	09.08.17 8:00	3.4e-5 Wm^{-2}	+166%	+150%	+208%	—	75	6
09.08.17 15:47 M2.9	75.14°	09.08.17 16:00	1.9e-5 Wm^{-2}	+91%	−50%	+20%	—	70	6
09.09.17 11:04 M3.7	35.67°	09.09.17 11:15	2.3e-5 Wm^{-2}	+103%	+76%	+176%	30 min	100	6
09.10.17 16:06 X8.2	79.34°	09.10.17 16:15	7.3e-4 Wm^{-2}	+172%	+213%	+243%	30 min	54	6

D- and E-layer seem to be larger than the electron density changes of the E-region itself.

The *fmin* parameter variation was between 0.4% and 283% at JR, 9% and 203% at PQ and 33% and 318% at VT during and after the investigated flare events. These detected *fmin* changes are in good agreement with the values measured at other European stations (Barta et al., 2019; 2022), in India (Sharma et al., 2010; Sripathi et al., 2013), in Japan (Tao et al., 2020) and in South America (Nogueira et al., 2015; Denardini et al., 2016) during and after M- and X-class flares. The observed changes depended on the intensity of the flare similarly to the results of Tao et al. (2020) and Barta et al. (2019). However, the solar zenith angle of the observation site also plays an important role, which agrees with the conclusion of Barta et al. (2019). These results are in good agreement with Mahajan et al. (2010) and Hazarika et al. (2016) who investigated the variation of total electron content (TEC: Total Electron Content) during intense solar flares and found a good correlation between the enhancement in TEC and increase in EUV flux, however, the local time of occurrence of the flares may also play an important role.

However, the neutral atmospheric circulation also can play a role in the local ionospheric anomalies observed at the different stations. E.g., at VT we observe an increase of *fmin* and similar change in absorption during the C8.3 (12:22 UT on 04. September) and X9.3 (12:02 UT on 06 September) flares, while at both PQ (50°N) and JR (54.6°N) we see higher attenuation during the X-class flare as expected. The neutral atmosphere above VT is influenced by different circulation patterns than the atmosphere above PQ and JR due to the location of Alpine massif and this fact can contribute to the different ionospheric responses. Regarding the model study of Pedatella and Liu (2018), a neutral atmosphere may significantly influence the behaviour of the ionosphere (variability leads to an uncertainty of typically 20%–40%, with localized regions exceeding 100%).

Based on our results, the *foF2* parameter measured during the investigated period is sensitive to the geomagnetic storm. A negative ionospheric storm can be clearly seen on the *foF2* variation during the main phase of the geomagnetic storm on 08 September (see D_{st} variation in Figure 2E) and the following night especially at JR, what is a sub-auroral station (please see Figures 4F, G). The decreased electron density appears also at PQ but it is not so pronounced at VT (please see Figures 4F–H). In parallel, if we look through the variation of the *fmin* parameter we can not recognise any changes of the diurnal pattern in connection with the geomagnetic storm, only the increased values at the time of the flare events are clear. It agrees well with the findings of previous studies, e.g., Barta et al., 2022, that the *fmin* parameter is sensitive to the changes caused by the solar flares, while the *foF2* parameter can show the variation caused by the dynamical changes in the thermosphere–ionosphere (F-region) system during geomagnetic storms.

The three different methods have their own advantages/disadvantages and their limitations. A common limitation of all the methods is that generally they can not be used during and right after the most intense solar flares (>M5) because there are no

measured data due to the generated total radio fade-out. The most intense X-class solar flares can produce clearly detectable changes in the Total Electron Content (TEC) derived from GNSS data (see e.g., Liu et al., 2004; Carrano et al., 2009; Zhang et al., 2011; Hernández-Pajares et al., 2012; Xiong et al., 2014). The advantage of the TEC data is that the GNSS measurements are not affected by the total radio fade-out. On the other hand, the impact of the less intense solar flares (<M5 class) is not that pronounced in TEC changes. Moreover, the effect of the flares can not be recognized during the presence of a strong geomagnetic storm (see Barta et al., 2022), because the TEC variation is more sensitive to the dynamical changes of the thermosphere–ionosphere (F-region) changes during geomagnetic storms. The described methods can be used as three different approaches to analyze the impact of the solar flares on the ionosphere and they can be beneficial despite their limitations.

The limitation of the amplitude method is that it can not be used at higher frequencies (>3.5 MHz) during the early morning hours and evening (and all of the night) when the value of the *foF2* drops below 3 MHz, because there is no reflection from the F-trace in these periods. This problem was particularly striking at the data measured at 4 MHz on the nights of the 08 and 09 September (see Figures 5C, D) during the investigated period. The *foF2* parameter decreased to ~2 MHz at JR and PQ (Figures 5F, G) indicating a negative ionospheric storm probably due to the geomagnetic storm (*Kp* = 8.3, Figure 2D, *Dst* ~ −100 nT; Figure 2E). This problem can be solved if in the analysis we also take into account the oblique traces during synchronized measurements with other ionosonde stations. Similar analyses on oblique sounding paths over longer distances could overcome this limitation. This can be a next step for future work. Moreover, when the *fmin* value is increased (>4–5 MHz) after the more intense solar flares (>M3 class) there are no detected amplitude data at the lower frequency band (2.5–3.5 MHz) because of the partial radio fade-outs which means a further limitation of the absorption method (see the results detailed in Section 3.1 and, e.g., Figures 6, 8, 10). Furthermore, it is difficult to determine which frequency is the best at the different stations to monitor the impact caused by the flares because the detected amplitude data at the different frequencies are highly variable based on the results (see e.g., Figure 10). Further limitation of the amplitude method is that it is difficult to estimate the magnitude of the caused effect based on that. Generally, very low amplitude values are detected in the early morning and evening hours. Therefore, the relative (percentage) change in absorption caused by the flare is large during these periods [see e.g., the impact of M3.2 flare occurred at 4:53 UT on 05 September, 740% changes at 2.5 MHz at JR (Table 2) and 1430% at VT (Table 4.)]. In contrast, around noon, when absorption is higher by default, the percentage change due to an intense flare is not as high. This is well demonstrated in the changes, e.g., after the X9.3 flare (peak time at 12:02 UT) on 06 September: 92% at 2.5 MHz at JR, 86% at PQ and only 77% at VT. This issue should be considered when evaluating the percentage result describing the ionospheric response. In summary, the method is well applicable in the lower frequency band during daytime (08–15 UT) after the less intense M-class flares (M1–M3) which do not cause total radio blackouts and very enhanced values of the *fmin* parameter.

The disadvantage of the *fmin* method is that the *fmin* parameter can depend on the background radio noise level, the radar characteristics and the other settings of the measurement, e.g., on the integration time (applying longer integration time (in standard 15 min mode) leading to lower *fmin* values, while lower integration time (used during campaign measurements, like the 2 min at PQ) resulting in higher *fmin* values). Consequently, the *fmin* method can be used only as a rough measure/indicator for the ionospheric absorption changes. It can be applied to investigate the relative changes: to compare the *fmin* parameter measured by the same system (preferably by the same settings) during flares and reference quiet days (e.g., Barta et al., 2019; 2022). On the other hand, the measurement of the *fmin* parameter is not limited by other ionospheric parameters (*foF2, foEs*) like in the above detailed case of the amplitude method. If there is a detected change in *fmin* value, it can be used as a rough measure of the ionospheric absorption during day and night.

The disadvantage of the SNR method is the saturation. The estimation of the caused effect is based on the ratio between the number of small values (<10 dB) and all the measured values at the investigated frequency ranges within 1 hour after the peak time of the flare (see Section 2.3). This gives an upper limit for the detected effect, because if all the observed values are zero or negligible during the one-hour period (total radio fade-out) it means 100%. Therefore, this limits the comparison of the effects caused by the most intense solar flares. The saturation issue of the SNR method can be solved by using a longer time period before and after the peak time of the flare for comparison. However, the applied time period should be selected carefully, because the larger solar flares (with longer duration) and their impact can overlap with each other. The effect of the geomagnetic storm can be seen on the SNR tables at all three investigated stations (please, see Supplementary Figures SA3A–C in the Supplementary Material). We can see a clear daily pattern at all stations on 04 September (left column on the Supplementary Figure SA3). Stronger signals in a wider frequency range (from approximately 2 to 6–7 MHz) during daytime (06:00–18:00 UT) and weaker signals in a smaller frequency range (1.5–4 MHz at VT, PQ, and 1–3 MHz at JR) in the evening and early morning hours. However, on 8 September the geomagnetic storm causes a negative ionospheric storm (decreased electron density) thus the maximum frequency became 5 MHz during daytime and can decrease below 2 MHz during the evening hours (it is especially pronounced at JR) which changes the daily pattern in the SNR table at the three stations (see Supplementary Figures SA3A–C in the Supplementary Material). Furthermore, the strength of the signal seems to be reduced on 8 September compared to the SNR measured on 04 September. Therefore, the geomagnetic activity should be taken into account when one would like to apply this method. Nevertheless, based on the present results (Tables 2–4) it seems an appropriate index to demonstrate the geoeffectiveness of a solar flare. The calculated changes (in %) depend on the intensity (class of the flare) and they seem to also show a solar zenith angle dependence. Furthermore, this method does not have limits like the amplitude method. Therefore, this method appears to be suitable to study the ionospheric absorption changes during solar flares, but it needs further investigation.

In the future, we plan to focus on the impact caused by the energetic particles (protons and electrons) accompanied by solar flares on the ionospheric absorption. They can have an important role in the sub-auroral region, like JR station. Another

step for future work can be to involve oblique traces recorded during synchronized measurements between two ionosondes into the analysis to overcome the issue related to the low *foF2* values during morning/late afternoon hours. Furthermore, we would like to compare the absorption changes calculated from different EM properties measured by the Digisondes (used in this paper) with other instruments which measure the ionospheric absorption, e.g., with the so-called A1 method (Bischoff and Taubenheim, 1967), or with riometer data. It will be also important to compare our results with the D-RAP model, commonly used to follow the changes in the ionospheric absorption globally. Moreover, we plan to study the geoeffectiveness of the investigated solar flares, namely how the changes (measured by the different methods) depend on the different properties of the flares, e.g., on solar zenith angle, on central meridian distance, or on the duration of the flare.

5 Conclusion

The present study demonstrates a novel method to determine the ionospheric absorption changes from amplitude data measured by European Digisondes (DPS-4D). The method has been applied to study the solar flare effects on the ionospheric absorption. The detected changes have been compared with the *fmin* parameter and the signal-to-noise ratio measured by the same Digisondes during the same events. Thirteen intense solar flares (>C8) have been selected for the investigation from the very active period of 04 and 10 September 2017. The solar zenith angle of the observation sites (to be <90°) was also considered during the selection. In order to compare the three methods used for the analysis of the ionospheric absorption variation, residuals have been defined for all parameters, which provide the percentage changes compared to the selected reference periods. The most important conclusions of the study are the followings:

- The amplitude changes measured at 2.5 MHz—which can be mainly related to the enhanced absorption occurring in the D-layer—varied between 68% and 1430% at the three European stations, Juliusruh, Průhonice and San Vito. The amplitude changes measured at 4 MHz—which indicate also the absorption variation in the E-region beside the D-layer—were between 18% and 565% at the three stations, thus a bit smaller than in the previous case. It agrees with the assumption that larger variations occurred in the D-layer after the solar flares than in the E-region.
- There are two main limitations of the amplitude method: 1) it can not be used at higher frequencies (>3.5 MHz) during the early morning hours and evening when the value of the *foF2* drops below 3 MHz; 2) there are no detected amplitude data at the lower frequency band (2.5–3.5 MHz) after the more intense solar flares (>M3 class) because of the partial radio fade-outs (*fmin* is increased above 4 MHz). Based on the results the method is well applicable in the lower frequency band during daytime (08–15 UT) after the less intense M-class flares (M1–M3) which do not cause total radio blackouts and very enhanced values of the *fmin* parameter. In future, we suggest utilization of oblique sounding as it allows for analysis of higher frequencies of the reflected signal.
- The variation of the *fmin* parameter was between 0.4% and 318% at the three stations during and after the investigated flare events. These detected fmin changes agree with the values measured in Europe and in other continents during and after M- and X-class flares based on the literature. The disadvantage of the *fmin* method is that the *fmin* parameter can depend on the background radio-noise level, the radar characteristics and the other settings of the measurement, e.g., on the integration time. However, it can be applied to investigate the relative changes (compare the *fmin* parameter measured during flares and reference quiet days) and it is not affected by other ionospheric parameters (*foF2*, *foEs*) like the amplitude method.
- The absorption changes detected by the SNR method were between 1% and 100% after the investigated flares. The caused effects are calculated by the ratio between the number of small values (<10 dB, also including missing values) and all the measured values at the investigated frequency ranges within 1 h after the peak time of the flare. Consequently, there is an upper limit (100%) for the detected effect. However, this method does not have other limitations like the amplitude method. Therefore, based on the present results this method appears to be suitable to study the geoeffectiveness of the solar flares on ionospheric absorption.

In summary, the combination of these three methods seems to be an efficient approach to monitor the ionospheric response to solar flares.

Data availability statement

Publicly available datasets were analyzed in this study. This data can be found here: The datasets presented in this study can be found in online repositories. The names of the repository/repositories and access number(s) are the following: Global Ionospheric Radio Observatory http://giro.uml.edu; NASA/GSFC's OMNI data set through OMNIWeb https://omniweb.gsfc.nasa.gov/; GOES 11 and 12 data, National Oceanic and Atmospheric Administration https://satdat.ngdc.noaa.gov/sem/goes/data/avg/; Hinode flare catalog https://hinode.isee.nagoya-u.ac.jp/flare_catalogue/; SAO-X software https://ulcar.uml.edu/SAO-X/SAO-X.html.

Author contributions

AB and VB conducted the scientific analysis of the data, produced the figures, and wrote the main part of the text. JM was responsible for the data from Juliusruh. DK, DB, ZM, and PK were responsible for the data from Pruhonice. All authors contributed to the article and approved the submitted version.

Funding

This work was supported by OTKA, Hungarian Scientific Research Fund (Grant No. PD 141967) of the National Research,

Development and Innovation Office. The contribution of VB was also supported by Bolyai Fellowship (GD, No. BO/00461/21) and by the GINOP-2.3.2-15-2016-00003 project. The authors appreciate support of the bilateral project of the Czech Academy of Sciences and Hungarian Academy of Sciences, title: Multiinstrumental investigation of the midlatitude ionospheric variability (n. MTA-19-03 and NKM 2018-28) in facilitating scientific communication. The work of the Czech team was also supported by the HORIZON 2020 PITHIA-NRF project (Grant Agreement No. 101007599).

Acknowledgments

The authors wish to express their gratitude to the late Gary Sales who made a substantial contribution in developing the absorption method used in this study and to Prof. Bodo Reinisch who attracted our attention to this method. The authors wish to thank the OMNIWeb data center for providing web access to the solar data of the Geostationary Operational Environmental Satellites (GOES) satellites.

Conflict of interest

The authors declare that the research was conducted in the absence of any commercial or financial relationships that could be construed as a potential conflict of interest.

Publisher's note

All claims expressed in this article are solely those of the authors and do not necessarily represent those of their affiliated organizations, or those of the publisher, the editors and the reviewers. Any product that may be evaluated in this article, or claim that may be made by its manufacturer, is not guaranteed or endorsed by the publisher.

Supplementary material

The Supplementary Material for this article can be found online at: https://www.frontiersin.org/articles/10.3389/fspas.2023.1201625/full#supplementary-material

References

Barta, V., Natras, R., Srećković, V., Koronczay, D., Schmidt, M., and Šulic, D. (2022). Multi-instrumental investigation of the solar flares impact on the ionosphere on 05-06 December 2006. *Front. Environ. Sci.* 10, 904335. doi:10.3389/fenvs.2022.904335

Barta, V., Sátori, G., Berényi, K. A., Kis, Á., and Williams, E. (2019). Effects of solar flares on the ionosphere as shown by the dynamics of ionograms recorded in Europe and South Africa. *Ann. Geophys.* 37 (4), 747–761. doi:10.5194/angeo-37-747-2019

Berdermann, J., Kriegel, M., Banyś, D., Heymann, F., Hoque, M. M., Wilken, V., et al. (2018). Ionospheric response to the X9.3 Flare on 6 September 2017 and its implication for navigation services over Europe. *Space weather.* 16, 1604–1615. doi:10.1029/2018SW001933

Berényi, K. A., Barta, V., and Kis, Á. (2018). Midlatitude ionospheric F2-layer response to eruptive solar events-caused geomagnetic disturbances over Hungary during the maximum of the solar cycle 24: A case study. *Adv. Space Res.* 61 (5), 1230–1243. doi:10.1016/j.asr.2017.12.021

Bilitza, D., Altadill, D., Truhlik, V., Shubin, V., Galkin, I., Reinisch, B., et al. (2017). International Reference Ionosphere 2016: From ionospheric climate to real-time weather predictions. *Space weather.* 15, 418–429. doi:10.1002/2016sw001593

Bischoff, K., and Taubenheim, J. (1967). A study of ionospheric pulse absorption (A1) on 4 Mc/s during the solar eclipse of May 20, 1966. *J. Atmos. solar-terrestrial Phys.* 29 (9), 1063–1069. doi:10.1016/0021-9169(67)90140-7

Buresova, D., Lastovicka, J., Hejda, P., and Bochnicek, J. (2014). Ionospheric disturbances under low solar activity conditions. *Adv. Space Res.* 54, 185–196. doi:10.1016/j.asr.2014.04.007

Carrano, C. S., Bridgwood, C. T., and Groves, K. M. (2009). Impacts of the December 2006 solar radio bursts on the performance of GPS. *Radio Sci.* 44, RS0A25. doi:10.1029/2008RS004071

Chen, J., Lei, J., Wang, W., Liu, J., Maute, A., Qian, L., et al. (2021). Ionospheric electrodynamic response to solar flares in September 2017. *J. Geophys. Res. Space Phys.* 126, e2021JA029745. doi:10.1029/2021JA029745

Curto, J. J., Marsal, S., Blanch, E., and Altadill, D. (2018). Analysis of the solar flare effects of 6 September 2017 in the ionosphere and in the Earth's magnetic field using Spherical Elementary Current Systems. *Space weather. J.* 16, 1709–1720. doi:10.1029/2018sw001927

Davies, K. (1990). *Ionospheric radio*. London Peregrinus.

Denardini, C. M., Resende, L. C. A., Moro, J., and Chen, S. S. (2016). Occurrence of the blanketing sporadic E layer during the recovery phase of the October 2003 superstorm. *Earth Planets Space* 68, 80. doi:10.1186/s40623-016-0456-7

Friis, H. T. (1946). A note on a simple transmission formula. *Proc. IRE* 34, 254–256. doi:10.1109/jrproc.1946.234568

George, P. L., and Bradley, P. A. (1973) Relationship between HF absorption at vertical and oblique incidence. *Proc. Inst. Electr. Eng.* 120, 1355–1361. doi:10.1049/piee.1973.0273

Handzo, R., Forbes, J. M., and Reinisch, B. (2014). Ionospheric electron density response to solar flares as viewed by digisondes. *Space weather.* 12, 205–216. doi:10.1002/2013sw001020

Hazarika, R., Kalita, B. R., and Bhuyan, P. K. (2016). Ionospheric response to X-class solar flares in the ascending half of the subdued solar cycle 24. *J. Earth Syst. Sci.* 125, 1235–1244. doi:10.1007/s12040-016-0726-6

Hernández-Pajares, M., García-Rigo, A., Juan, J. M., Sanz, J., Monte, E., Aragón-Àngel, A., et al. (2012). GNSS measurement of EUV photons flux rate during strong and mid solar flares. *Space weather.* 10 (12). doi:10.1029/2012sw000826

Higashimura, M., Sinno, K., and Hirukawa, Y. (1969a). Analysis of long-term observations of ionospheric absorption measurement (I). Observations at kokubunji. *J. Radio Res. Lab.* 16, 131–138.

Higashimura, M., Sinno, K., and Hirukawa, Y. (1969b). Analysis of long-term observations of ionospheric absorption measurement (II). Observations in the northern hemisphere. *J. Radio Res. Lab.* 16, 139–147.

Kokourov, V. D., Vergasova, G. V., and Kazimirovsky, E. S. (2006). Longterm variations of ionospheric parameters as a basis for the study of the upper-atmospheric climate. *Phys. Chem. Earth, PartsA/B/C* 31.1, 54–58. doi:10.1016/j.pce.2005.03.002

Kolarski, A., Veselinović, N., Srećković, V. A., Mijić, Z., Savić, M., and Dragić, A. (2023). Impacts of extreme space weather events on september 6th, 2017 on ionosphere and primary cosmic rays. *Remote Sens.* 15 (5), 1403. doi:10.3390/rs15051403

Little, C. G. (1954). High latitude ionospheric observations using extra-terrestrial radio waves. *Proc. IRE* 42, 1700. doi:10.1016/0021-9169(95)00072-0

Liu, J., Qian, L., Maute, A., Wang, W., Richmond, A. D., Chen, J., et al. (2021a). Electrodynamical coupling of the geospace system during solar flares. *J. Geophys. Res. Space Phys.* 125, e2020JA028569. doi:10.1029/2020JA028569

Liu, J., Wang, W., Qian, L., Lotko, W., Burns, A. G., Pham, K., et al. (2021b). Solar flare effects in the Earth's magnetosphere. *Nat. Phys.* 17 (7), 807–812. doi:10.1038/s41567-021-01203-5

Liu, J. Y., Lin, C. H., Tsai, H. F., and Liou, Y. A. (2004). Ionospheric solar flare effects monitored by the ground-based GPS receivers: Theory and observation. *J. Geophys. Res.* 109, A01307. doi:10.1029/2003JA009931

Liu, X., Liu, J., Wang, W., Zhang, S.-R., Zhang, K., Lei, J., et al. (2022). Explaining solar flare-induced ionospheric ion upflow at Millstone Hill (42.6°N.). *J. Geophys. Res. Space Phys.* 127, e2021JA030185. doi:10.1029/2021JA030185

Mahajan, K. K., Lodhi, N. K., and Upadhayaya, A. K. (2010). Observations of X-ray and EUV fluxes during X-class solar flares and response of upper ionosphere. *J. Geophys. Res. Space Phys.* 115 (A12). doi:10.1029/2010ja015576

Mosna, Z., Kouba, D., Knizova, P. K., Buresova, D., Chum, J., Sindelarova, T., et al. (2020). Ionospheric storm of September 2017 observed at ionospheric station Pruhonice, the Czech Republic. *Adv. Space Res.* 65 (1), 115–128. doi:10.1016/j.asr.2019.09.024

Nogueira, P. A. B., Souza, J. R., Abdu, M. A., Paes, R. R., Sousasantos, J., Marques, M. S., et al. (2015). Modeling the equatorial and low-latitude ionospheric response to an intense X class solar flare. *J. Geophys. Res. Space Phys.* 120, 3021–3032. doi:10.1002/2014ja020823

Oksman, J., Wagner, C. U., Kaila, K., and Lauter, A. E. (1981). Post-storm mid-latitude green aurora and electron precipitation. *Planet. Space Sci.* 29, 405–413. doi:10.1016/0032-0633(81)90084-2

de Paula, V., Segarra, A., Altadill, D., Curto, J. J., and Blanch, E. (2022). Detection of solar flares from the analysis of signal-to-noise ratio recorded by Digisonde at mid-latitudes. *Remote Sens.* 14, 1898. doi:10.3390/rs14081898

Pedatella, N. M., and Liu, H.-L. (2018). The influence of internal atmospheric variability on the ionosphere response to a geomagnetic storm. *Geophys. Res. Lett.* 45, 4578–4585. doi:10.1029/2018GL077867

Ratcliffe, J. A. (1972). *An introduction to the ionosphere and magnetosphere*. Cambridge: The University Press.

Reinisch, B. W., and Galkin, I. A. (2011). Global ionospheric radio observatory (GIRO). *Earth Planet Sp.* 63, 377–381. doi:10.5047/eps.2011.03.001

Rishbeth, H., and Garriot, O. K. (1969). Introduction to ionospheric Physics, *Int. Geophys. Ser*, Vol. 14, Academic Press, NY, 87–120.

Rose, D. C., and Ziauddin, S. (1962). The polar cap absorption effect. *Space Sci. Rev.* 1, 115–134. doi:10.1007/bf00174638

Sales, G. S. (2011). *HF absorption measurements using routine digisonde data*, Conference material, XII. Lowell, MA: International Digisonde Forum, University of Massachusetts.

Sauer, H. H., and Wilkinson, D. C. (2008). Global mapping of ionospheric HF/VHF radio wave absorption due to solar energetic protons. *Space weather.* 6, 12002. doi:10.1029/2008SW000399

Schmitter, E. D. (2011). Remote sensing planetary waves in the midlatitude mesosphere using low frequency transmitter signals. *Ann. Geophys.* 29, 1287–1293. doi:10.5194/angeo-29-1287-2011

Scotto, C., and Settimi, A. (2014). The calculation of ionospheric absorption with modern computers. *Adv. Space Res.* 54 (8), 1642–1650. doi:10.1016/j.asr.2014.06.017

Sharma, S., Chandra, H., Vats, H. O., Pandya, N. Y., and Jain, R. (2010). Ionospheric modulations due to solar flares over Ahmedabad. *Indian J. Radio Space Phys.* 39, 296–301.

Srećković, V. A., Šulić, D. M., Ignjatović, L., and Vujčić, V. (2021). Low ionosphere under influence of strong solar radiation: Diagnostics and modeling. *Appl. Sci. (Basel).* 11 (16), 7194. doi:10.3390/app11167194

Sripathi, S., Balachandran, N., Veenadhari, B., Singh, R., and Emperumal, K. (2013). Response of the equatorial and low-latitude ionosphere to an intense X-class solar flare (X7/2B) as observed on 09 August 2011. *J. Geophys. Res. Space Phys.* 118, 2648–2659. doi:10.1002/jgra.50267

Stauning, P. (1996). Investigations of ionospheric radio wave absorption processes using imaging riometer techniques. *J. Atmos. solar-terrestrial Phys.* 58 (6), 753–764. doi:10.1016/0021-9169(95)00072-0

Šulić, D. M., and Srećković, V. A. (2014). A comparative study of measured amplitude and phase perturbations of VLF and LF radio signals induced by solar flares. *Serb. Astron. J.* 188, 45–54. doi:10.2298/saj1488045s

Šulić, D. M., Srećković, V. A., and Mihajlov, A. A. (2016). A study of VLF signals variations associated with the changes of ionization level in the D-region in consequence of solar conditions. *Adv. Space Res.* 57, 1029–1043. doi:10.1016/j.asr.2015.12.025 1029–

Tao, C., Nishioka, M., Saito, S., Shiota, D., Watanabe, K., Nishizuka, N., et al. (2020). Statistical analysis of short-wave fadeout for extreme space weather event estimation. *Earth, Planets Space* 72, 173. doi:10.1186/s40623-020-01278-z

Tsurutani, B. T., Verkhoglyadova, O. P., Mannucci, A. J., Lakhina, G. S., Li, G., Zank, G. P., et al. (2009). A brief review of "solar flare effects" on the ionosphere. *Radio Sci.* 44, 1–14. doi:10.1029/2008rs004029

Xiong, B., Wan, W., Ning, B., Ding, F., Hu, L., Yu, Y., et al. (2014). A statistic study of ionospheric solar flare activity indicator. *Space weather.* 12, 29–40. doi:10.1002/2013SW001000

Yasyukevich, Y., Astafyeva, E., Padokhin, A., Ivanova, V., Syrovatskii, S., and Podlesnyi, A. (2018). The 6 September 2017 X-class solar flares and their impacts on the ionosphere, GNSS, and HF radio wave propagation. *Space weather.* 16 (8), 1013–1027. doi:10.1029/2018sw001932

Zhang, D. H., Mo, X. H., Cai, L., Zhang, W., Feng, M., Hao, Y. Q., et al. (2011). Impact factor for the ionospheric total electron content response to solar flare irradiation. *J. Geophys. Res. Space Phys.* 116 (A4). doi:10.1029/2010ja016089

Zolesi, B., and Cander, L. (2014). *Ionospheric prediction and forecasting*. New York Dordrecht London: Springer Geophysics, Springer Heidelberg, 33–43.